doi.org/10.1002/cbdv.202301063 Research Article CHEMISTRY & BIODIVERSITY

www.cb.wiley.com

Synthesis, Theoretical, *in Silico* and *in Vitro* Biological Evaluation Studies of New Thiosemicarbazones as Enzyme Inhibitors

Musa Erdoğan,[a] M. Serdar Çavuş,[b] Halit Muğlu,[c] Hasan Yakan,*[d] Cüneyt Türkeş,[e] Yeliz Demir,*[f] and Şükrü Beydemir[g, h]

Eleven new thiosemicarbazone derivatives (**1**–**11**) were designed from nine different biologically and pharmacologically important isothiocyanate derivatives containing functional groups such as fluorine, chlorine, methoxy, methyl, and nitro at various positions of the phenyl ring, in addition to the benzyl unit in the molecular skeletal structure. First, their substituted-thiosemicarbazide derivatives were synthesized from the treatment of isothiocyanate with hydrazine to synthesize the designed compounds. Through a one-step easy synthesis and an eco-friendly process, the designed compounds were synthesized with yields of up to 95% from the treatment of the thiosemicarbazides with aldehyde derivatives having methoxy and hydroxy groups. The structures of the synthesized molecules were elucidated with elemental analysis and FT–IR, ^{1}H-NMR, and ^{13}C-NMR spectroscopic methods. The electronic and spectroscopic properties of the compounds were determined by the DFT calculations performed at the B3LYP/6-311++G(2d,2p) level of theory, and the experimental findings were supported. The effects of some global reactivity parameters and nucleophilic-electrophilic attack abilities of the compounds on the enzyme inhibition properties were also investigated. They exhibited a highly potent inhibition effect on acetylcholinesterase (AChE) and carbonic anhydrases (*h*CAs) (K_I values are in the range of 23.54±4.34 to 185.90±26.16 nM, 103.90±23.49 to 325.90±77.99 nM, and 86.15±18.58 to 287.70±43.09 nM for AChE, *h*CA I, and *h*CA II, respectively). Furthermore, molecular docking simulations were performed to explain each enzyme-ligand complex's interaction.

Introduction

The compounds containing Schiff bases have biological and medicinal properties with wide range of applications, such as antimicrobial,[1] antifungal,[2] antiproliferative activity and enzyme inhibition,[3,4] anticonvulsant,[5] antituberculosis,[6] anticancer,[7] anti-inflammatory,[8] antioxidant,[9] and antibacterial[10] activity. Thiosemicarbazones with the –NH–C(=S)NH–N= unit constitute a versatile class of synthetic organic chemistry. They are also used as versatile intermediates for synthesizing numerous compounds. They have shown a broad spectrum of chemical, biological and medicinal properties such as anti-HIV,[11] antimicrobial[12] antiviral,[13] antibacterial,[14] anticonvulsant,[15] anticancer,[16] urease inhibitory activity,[17] antituberculosis,[18] cytotoxic activity,[19] and antioxidant agents.[20–22]

The ubiquitous enzyme superfamily of carbonic anhydrases (CAs; EC 4.2.1.1) plays a crucial role in most organisms/tissues due to its involvement in numerous physiologic and pathologic processes.[23] This is because it catalyzes the reaction that converts CO_2 into bicarbonate and protons, which is a straightforward but crucial reaction.[24] Eight genetically different CA families are being recognized, and as they are expressed in animals from all branches of the evolutionary tree, they can be targeted by various illnesses. In particular, CA inhibitors (CAIs) emerged as useful tools in diseases typically not

[a] *Dr. M. Erdoğan*
Department of Food Engineering, Faculty of Engineering and Architecture, Kafkas University, 36100 Kars, Turkey

[b] *Dr. M. Serdar Çavuş*
Department of Biomedical Engineering, Faculty of Engineering and Architecture, Kastamonu University, 37200 Kastamonu, Turkey

[c] *Dr. H. Muğlu*
Department of Chemistry, Faculty of Sciences, Kastamonu University, 37200 Kastamonu, Turkey

[d] *Dr. H. Yakan*
Department of Chemistry Education, Faculty of Education, Ondokuz Mayis University, 55200 Samsun, Turkey
E-mail: hasany@omu.edu.tr

[e] *Dr. C. Türkeş*
Department of Biochemistry, Faculty of Pharmacy, Erzincan Binali Yıldırım University, 24002 Erzincan, Turkey

[f] *Dr. Y. Demir*
Department of Pharmacy Services, Nihat Delibalta Göle Vocational High School, Ardahan University, 75700 Ardahan, Turkey
E-mail: yelizdemir@ardahan.edu.tr

[g] *Prof. Ş. Beydemir*
Department of Biochemistry, Faculty of Pharmacy, Anadolu University, 26470 Eskişehir, Turkey

[h] *Prof. Ş. Beydemir*
Bilecik Şeyh Edebali University, 11230 Bilecik, Turkey
Department of Chemistry Education, Faculty of Education, Ondokuz Mayis University, Samsun 55200, Turkey

Supporting information for this article is available on the WWW under https://doi.org/10.1002/cbdv.202301063

associated with this class of pharmacological agents, such as oxidative stress, as an anti-infective agent, Alzheimer's disease (AD), neuropathic pain, cerebral ischaemia, and rheumatoid arthritis in the last decades.[25] They also found clinical relevance as antiobesity, antiglaucoma drugs, diuretics, antitumor, and antiepileptics agents.[26]

A cholinergic enzyme called acetylcholinesterase (AChE) is mainly present in postsynaptic neuromuscular junctions, especially in nerves and muscles. A natural neurotransmitter called acetylcholine (ACh) is quickly degraded into acetic acid and choline.[27] The primary role of AChE is to inhibit synaptic transmission and communication between neurons to prevent ACh from activating and spreading nearby receptors. The only class of medications expressly used to treat AD are cholinergic enhancers called AChE inhibitors.[28] AChE inhibitors have a neuroprotective effect on the activation of nicotinic receptors and muscarinic receptors, which improves cognitive function by slowing the decline of ACh in the synaptic cleft and increasing the concentration of an ACh in these receptors.[29] Therefore, there is a need for the synthesis of promising new compounds that inhibit the AChE enzyme in the treatment of AD disease.[30] There are many organic compounds in the literature have been tested in the effects of on the inhibition of CAs and AChE enzymes.[31–35] In our former work, thiosemicarbazone derivatives exhibited highly potent inhibition of AChE and *h*CAs. All compounds showed lower activity than reference drug acetazolamide (AAZ) for *h*CA I (Scheme 1a). The most active *N*-(2-chlorophenyl)-2-(4-hydroxy-3,5-dimethoxybenzylidene)hydrazine-1-carbothioamide showed with K_I values of 60.32 ± 9.78 nM.[31] In our other work, thiosemicarbazones bearing the Schiff base showed highly potent inhibition effect with K_I values are in the range of 51.11–78.10 nM for AChE, 60.32–300.00 nM for *h*CA I, and 64.21–307.70 nM, for *h*CA II (Scheme 1b).[32] In another work, thiosemicarbazone derivatives based 3-ethoxysalicylaldehyde assayed against carbonic anhydrases (hCA I and hCA II), cholinesterases (AChE and BChE) and α-glycosidase (Scheme 1c). The results existing they effectively inhibited AChE, with K_I values in the range of 385.38 ± 45.03 to 983.04 ± 104.64 nM.[34]

With the above considerations in mind, we designed new thiosemicarbazone derivatives containing biologically and pharmacologically important units in their hybrid structure and decided to examine their enzyme-inhibitory properties to discover potential enzyme inhibitors (against AChE, *h*CA I, and *h*CA II). For this, nine different thiosemicarbazide derivatives were first synthesized from the reaction of various substituted isothiocyanate derivatives with hydrazine. When choosing isothiocyanate derivatives, in addition to the benzyl derivative, derivatives containing important groups in terms of biological activity, such as methyl, nitro, fluorine, chlorine, and methoxy in different positions of the phenyl ring, were preferred. Then, the new thiosemicarbazones bearing Schiff-bases (**1-11**) were accomplished by condensation reaction with 3-methoxy or 4-hydroxy salicylicaldehyde and with various substituted-thiosemicarbazides under reflux in ethanol. The structures of the compounds were characterized by Fourier transform infrared (FT–IR), proton–carbon nuclear magnetic resonance (^{1}H-NMR – ^{13}C-NMR), and elemental analysis. Experimental spectroscopy results were compared with density functional theory (DFT) data calculated at the B3LYP/6-311 + + g(2d,2p) level of theory. In addition to calculating the global reactivity parameters of compounds, the effects of substituents on the intramolecular interactions and electronic properties of compounds have been investigated using the *interaction region indicator* (IRI) and *quantum theory of atoms in molecules* (QTAIM) analyses. An examination of the enzyme inhibition characteristics of the compounds and their relationship with possible nucleophilic and electrophilic attacks was carried out on electronic data, and as a result, some predictions were made about the sources of the enzyme inhibition properties of the compounds. Besides, molecular docking studies were accomplished to explain each enzyme-ligand complex's interaction. Moreover, although there are studies on biological activities using DFT and docking approaches in the literature,[35] our study focuses more on predicting how substituent groups and the positions of these

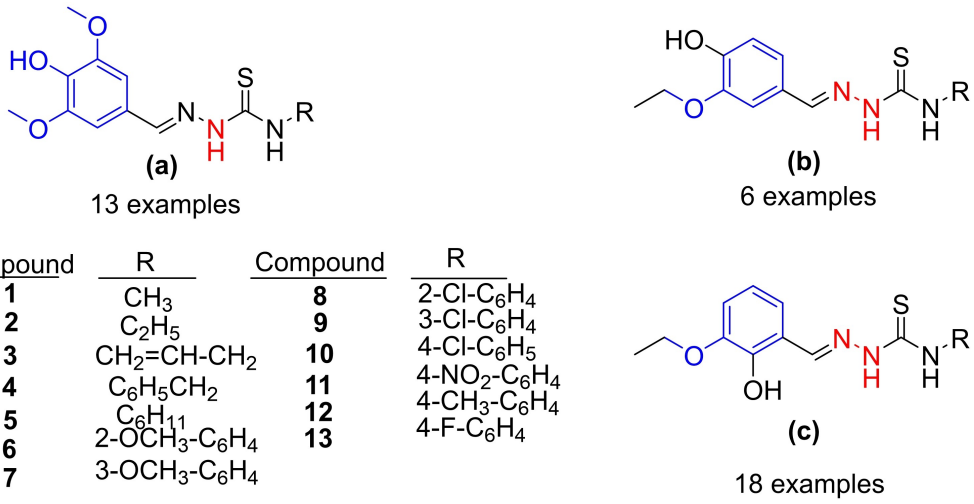

Compound	R	Compound	R
1	CH_3	8	2-Cl-C_6H_4
2	C_2H_5	9	3-Cl-C_6H_4
3	CH_2=CH-CH_2	10	4-Cl-C_6H_5
4	$C_6H_5CH_2$	11	4-NO_2-C_6H_4
5	C_6H_{11}	12	4-CH_3-C_6H_4
6	2-OCH_3-C_6H_4	13	4-F-C_6H_4
7	3-OCH_3-C_6H_4		

Scheme 1. Structures of thiosemicarbazones bearing Schiff-bases as CAs and AChE inhibitors.

groups affect enzyme inhibition through electrophilic/nucleophilic attacks.

Results and Discussion

Physical properties

The structure names, yields, melting points, physical properties, and elemental analyses data of the compounds are given in Tables 1 and 2.

Vibrational frequencies

In the FT-IR spectra of the compounds, the vibrations of the aldehyde group (–CHO, 2 bands) and the amino group ($–NH_2$) of the starting material did not detect at 2800–2650 cm^{-1} and 3350–3200 cm^{-1}, respectively. Instead, new for the –C=N stretching vibrations of azomethine group were observed at 1629–1579 cm^{-1}. These frequencies indicated a successful reaction as expected (see Figures S1-S11 in Supplementary information for the spectra of the compounds).

For the compounds (**1**–**11**), the hydroxy group (–OH) vibration peaks were observed in the range 3405–3292 cm^{-1}, the amine group (–NH) vibration peaks were observed in the range 3293–3107 cm^{-1}, aromatic proton (–CH) vibrations were observed in the range 3080–2934 cm^{-1}, the –C=S signals of the thiosemicarbazone region were observed at 1478–1437 cm^{-1}, the –C–N group vibrations were observed at 1311–1213 cm^{-1}, and the –C–O group vibrations were observed at 1215–1025 cm^{-1}.

For compound **3**, the asymmetric and symmetric stretching vibrations of the nitro group ($–NO_2$) were not observed at 1498 and 1337 cm^{-1}. For compounds **4** and **7**, Ar–F vibration signal was observed at 1216 and 1138 cm^{-1}, respectively. For the compounds **5** and **8**, the –C–Cl stretching vibrations were observed at 912 and 928 cm^{-1}, respectively. The experimental and calculated IR vibration values of the compounds are given in Table 3. The stretching vibration data of all structures were compatible with those reported for similar compounds.[20,36]

^{1}H-NMR interpretations

NMR spectra were recorded on a Bruker Ultrashield Plus Biospin spectrometer at 400 MHz in DMSO-d_6. NMR chemical shifts were determined relative to internal standard TMS at δ 0.0 ppm. Chemical shifts (δ) are reported in ppm, and coupling constants (J) are in Hertz (Hz). The experimental and calculated ^{1}H-NMR spectrum values of the compounds are given in Tables 4a and 4b. Signals of DMSO-d_6 and water in DMSO (HOD, H_2O) were observed around 2.00, 2.55 (quintet), and 3.40 (variable, depending on the solvent and its concentration) ppm in ^{1}H-NMR, and 39–41 ppm (heptet peaks) in ^{13}C-NMR, respectively.

In the ^{1}H-NMR characterization of the synthesized compounds, the amino peaks of the thiosemicarbazide units (N–N*H*–C=S, H5) in **1**–**11** were observed as a sharp singlet between 12.17–11.35 ppm. The azomethine protons (C*H*=N) of the compounds, one of the most specific peaks, were resonated as a singlet at the range of 8.55-8.31 ppm. A characteristic singlet signal was also observed at around 10.40-9.42 ppm assigned to the OH protons in the 2-hydroxyphenyl ring of all the compounds. For compounds **10**–**11**, the free OH peaks at *para* position of 2,4-dihydroxyphenyl ring were appeared as a singlet at 9.86 ppm for **10**, and 9.77 ppm for **11**. The presence of H6 protons at aniline units was indicated for all the compounds. Furthermore, for the compounds **1**–**9**, the aromatic ring protons (H1, H2, and H3) were resonated as a doublet of doublets at 7.02–6.99 ppm (J=8.0–8.1), a triplet at 6.86–6.78 ppm (J=8.0), and a doublet at 7.72–7.51 ppm (J=8.0-7.6), respectively. For the compound **10**, the aromatic ring protons (H1 and H2) were resonated as multiplets at 6.40–6.28 ppm, and H3 protons were resonated as doublet at 7.67 ppm (J=8.2). For the compound **11**, the aromatic ring protons (H1 and H2) were resonated as doublet at 6.32 ppm (J=2.3), a doublet of doublets at 6.28 ppm (J=8.5) and H3 protons were resonated as doublet at 7.74 ppm (J=8.6) (see Figures S12–S22). The aromatic ring protons in aniline unit gave AB system for the compounds **2** and **3** in ^{1}H-NMR spectra (see Figures S13 and S14). The other NMR signals which observed at the aromatic and aliphatic regions are in agreement with the molecular structures for the related compounds. These results consistent with the values of earlier reported for similar compounds.[3,20,22,37]

^{13}C-NMR interpretations

The experimental and calculated ^{13}C-NMR spectrum values of the compounds are given in Tables 5a and 5b. In ^{13}C-NMR for all the compounds **1**–**11**, the characteristic signal of thiosemicarbazide units (*C*=S) was observed at the most downfield (It appears between 177.43–173.88 ppm). On the other hand, the characteristic imine signals (*C*=N) were showed between 141.16–139.40 ppm. Other ^{13}C-NMR chemical shift values which observed in the aromatic and aliphatic regions supported the formation of compounds **1**–**11** (for details see Figures S12–S22 in Supplementary Information). In the ^{19}F-decoupled ^{13}C-NMR spectrum, C–F couplings were observed in the compounds **4** and **7**, as expected. Fluorophenyl carbons resonated as doublets at 157.15 (d, J=246.5, C8), 129.90 (s, C11) 127.88 (d, J=7.8, C10), 127.25 (d, J=11.8, C7), 123.91 (d, J=3.5, C12), 115.58 (d, J=20.0, C9) ppm for the compound **4**, and 161.50 (d, J=241.6, C9), 140.90 (d, J=10.9, C7), 129.42 (d, J=9.3, C11), 121.04 (s, C12), 111.95 (d, J=24.7,C8), 111.53 (d, J=20.9, C10) for the compound **7**, respectively. The NMR data are in very good agreement with the structure of targeted the compounds and are in consistent with reported similar compounds in the literature.[3,20,22,37]

Table 1. Structural and physical properties of the compounds.

Comp. ID	Structure	Structure Name	Yield %	M. P. (°C)	Color
1	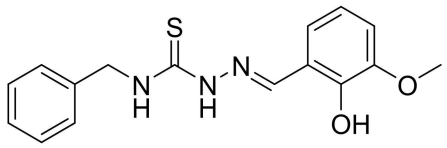	*N*-benzyl-2-(2-hydroxy-3-methoxybenzylidene)hydrazine-1-carbothioamide	93	202–203	White
2	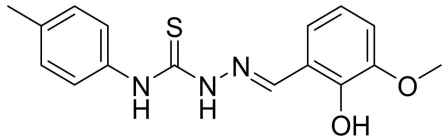	*N*-(*p*-tolyl)-2-(2-hydroxy-3-methoxybenzylidene)hydrazine-1-carbothioamide	92	208–209	White
3	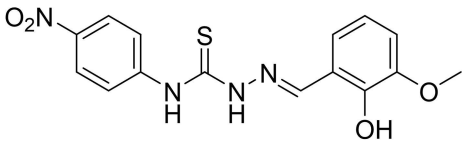	*N*-(4-nitrophenyl)-2-(2-hydroxy-3-methoxybenzylidene)hydrazine-1-carbothioamide	94	213–214	Yellow
4	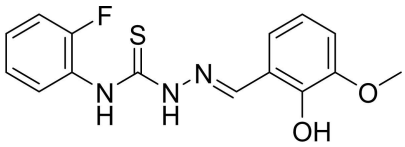	*N*-(2-fluorophenyl)-2-(2-hydroxy-3-methoxybenzylidene)hydrazine-1-carbothioamide	78	185–186	White
5	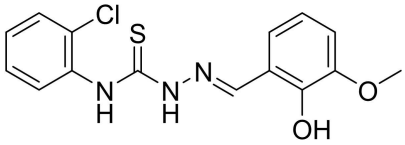	*N*-(2-chlorophenyl)-2-(2-hydroxy-3-methoxybenzylidene)hydrazine-1-carbothioamide	85	202–203	White
6	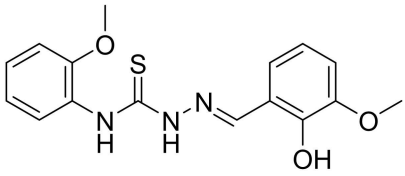	*N*-(2-methoxyphenyl)-2-(2-hydroxy-3-methoxybenzylidene)hydrazine-1-carbothioamide	75	186–187	Yellowish White
7	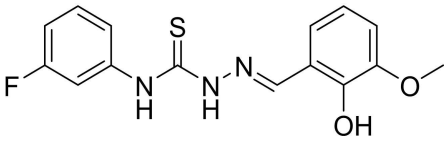	*N*-(3-fluorophenyl)-2-(2-hydroxy-3-methoxybenzylidene)hydrazine-1-carbothioamide	68	199–200	White
8	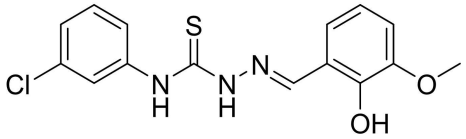	*N*-(3-chlorophenyl)-2-(2-hydroxy-3-methoxybenzylidene)hydrazine-1-carbothioamide	88	194–195	White
9	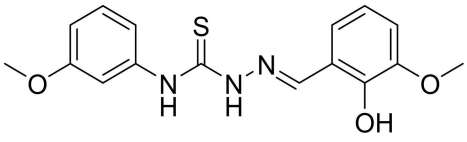	*N*-(3-methoxyphenyl)-2-(2-hydroxy-3-methoxybenzylidene)hydrazine-1-carbothioamide	95	196-197	White
10	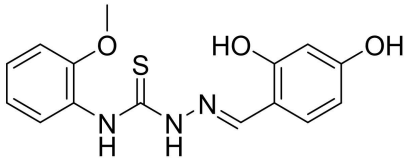	*N*-(2-methoxyphenyl)-2-(2,4-dihydroxybenzylidene)hydrazine-1-carbothioamide	73	210–211	Light Yellow

Table 1. continued

Comp. ID	Structure	Structure Name	Yield %	M. P. (°C)	Color
11	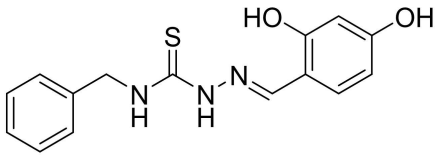	*N*-benzyl-2-(2,4-dihydroxybenzylidene)hydrazine-1-carbothioamide	78	208–209	Yellowish White

Table 2. Elemental analysis results of the compounds.

Comp. ID	Molecular mass (g/mol)	Molecular formula	Calculated			Experimental		
			C%	H%	N%	(C)%	(H)%	(N)%
1	315.39	$C_{16}H_{17}N_3O_2S$	60.93	5.43	13.32	61.01	5.38	13.36
2	315.39	$C_{16}H_{17}N_3O_2S$	60.93	5.43	13.32	60.85	5.47	13.30
3	346.36	$C_{15}H_{14}N_4O_4S$	52.02	4.07	16.18	51.94	4.01	16.25
4	319.35	$C_{15}H_{14}FN_3O_2S$	56.42	4.42	13.16	56.52	4.39	13.12
5	335.81	$C_{15}H_{14}ClN_3O_2S$	53.65	4.20	12.51	53.56	4.23	12.47
6	331.34	$C_{16}H_{17}N_3O_3S$	57.99	5.17	12.68	58.08	5.12	12.63
7	319.35	$C_{15}H_{14}FN_3O_2S$	56.42	4.42	13.16	56.51	4.45	13.14
8	335.81	$C_{15}H_{14}ClN_3O_2S$	53.65	4.20	12.51	53.60	4.16	12.55
9	331.34	$C_{16}H_{17}N_3O_3S$	57.99	5.17	12.68	57.95	5.24	12.70
10	317.36	$C_{15}H_{15}N_3O_3S$	56.77	4.76	13.24	56.67	4.68	13.29
11	301.36	$C_{15}H_{15}N_3O_2S$	59.78	5.02	13.94	59.71	5.08	14.00

Table 3. Experimental and calculated FT-IR values of the compounds (cm^{-1}).

	Comp. ID	-OH	-NH	Ar.CH	C=N	C=S	C-N	C–O (OH)	C–O (OCH_3)	Spec. Vib.
Experimental	**1**	3304	3214, 3143	3037–2983	1579	1355	1215	1185	1063	–
	2	3298	3201, 3137	3071–2998	1585	1358	1275	1184	1068	–
	3	3337	3280, 3218	3080–2985	1598	1405	1224	1188	1054	NO_2: 1498, 1337
	4	3296	3255, 3127	3008–2935	1591	1424	1267	1215	1057	C–F: 1216
	5	3306	3273, 3177	3013–2934	1587	1358	1226	1190	1059	C–Cl: 912
	6	3297	3269, 3145	3056–2960	1598	1406	1235	1159	1070,1025	–
	7	3292	3201, 3107	3066–3002	1595	1356	1269	1201	1068	C–F: 1138
	8	3296	3211, 3135	3004–2971	1580	1401	1272	1190	1067	C–Cl: 928
	9	3403	3293, 3121	3075–2967	1597	1358	1215	1162	1062, 1032	–
	10	3317	3243, 3189	3018–2971	1603	1349	1237	1163,1119	1037	–
	11	3405	3286, 3169	3023–2991	1629	1358	1311	1159,1113	1114	–
Calculated	**1**	3776	3587, 3532	3215–3159	1656	1438	1225	1245	1089	–
	2	3775	3532, 3526	3236–3154	1648	1431	1268	1245	1089	–
	3	3772	3530, 3515	3240–3173	1649	1422	1283	1247	1087	NO_2: 1551, 1354
	4	3773	3530, 3519	3236–3187	1649	1428	1277	1246	1089	C–F: 1224
	5	3774	3528, 3488	3230–3187	1649	1426	1274	1255	1089	C–Cl: 1050
	6	3775	3528, 3515	3234–3184	1648	1432	1271	1245	1089, 1054	–
	7	3773	3531, 3524	3243–3185	1648	1427	1284	1246	1089	C–F: 1218
	8	3773	3531, 3522	3241–3184	1648	1426	1266	1246	1088	C–Cl: 988
	9	3774	3532, 3527	3247–3179	1648	1430	1237	1247	1089, 1067	–
	10	3838, 3835	3531, 3518	3234–3167	1646	1432	1273	1224	1054	–
	11	3838, 3834	3577, 3538	3194–3161	1645	1437	1333	1224	–	–

Table 4. a) Experimental ^{1}H-NMR (δ, ppm, in (D_6)DMSO) values of the compounds. b) Calculated ^{1}H-NMR values of the compounds

a)

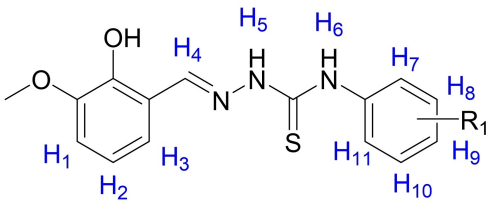

1-9

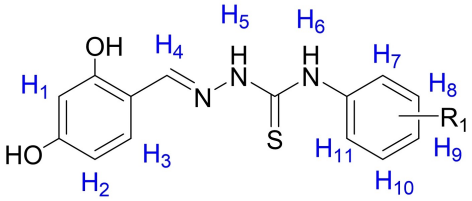

10-11

Comp. ID	OH	OCH_3/ OH	H1	H2	H3	H4, CH=N	H5, NH	H6, NH-Ar	H7-H11	R_1
1	9.22 (s, 1H)	3.81 (s, 3H)	6.96 (dd, *J*=8.1, 1.4, 1H)	6.78 (t, *J*=8.0, 1H)	7.59 (d, *J*=8.0, 1H)	8.47 (s, 1H)	11.59 (s, 1H)	9.01 (t, *J*=6.2, 1H)	7.47–7.16 (m, 5H, benzyl H7-H11)	CH_2: 4.85 (d, *J*=6.2, 2H)
2	9.96 (s, 1H)	3.82 (s, 3H),	6.98 (dd, *J*=8.0, 1.3, 1H),	6.79 (t, *J*=8.0, 1H)	7.70 (d, *J*=7.9, 1H)	8.51 (s, 1H)	11.75 (s, 1H)	9.25 (bs, 1H)	7.43 (d, *J*=8.3, 2H, H7, H11, H7=H11), 7.16 (d, *J*=8.3, 2H, H8, H10, H8=H10)	H9=CH_3: 2.31 (s, 3H)
3	10.40 (s, 1H)	3.84 (s, 3H)	7.02 (dd, *J*=8.1, 1.3, 1H),	6.83 (t, *J*=8.0, 1H),	7.72 (d, *J*=7.6, 1H),	8.59 (s, 1H)	12.17 (s, 1H)	9.35 (bs, 1H)	8.25 (d, *J*=9.2, 2H, H8, H10, H8=H10), 8.08 (d, *J*=9.2, 2H, H7, H11, H7=H11)	H9=NO_2
4	9.91 (s, 1H)	3.82 (s, 3H)	6.99 (dd, *J*=8.0, 1.3, 1H)	6.79 (t, *J*=8.0, 1H),	7.68 (d, *J*=7.8, 1H)	8.52 (s, 1H)	11.95 (s, 1H)	9.26 (bs, 1H)	7.55 (t, *J*=7.9, 1H, H11), 7.43–7.13 (m, 3H, H8, H9, H10)	H7=F
5	10.03 (s, 1H)	3.83 (s, 3H)	6.99 (dd, *J*=8.0, 1.3, 1H)	6.80 (t, *J*=8.0, 1H)	7.64 (d, *J*=7.8, 1H)	8.54 (s, 1H)	11.98 (s, 1H)	9.28 (bs, 1H)	7.80 (dd, *J*=7.9, 1.3, 1H, H11), 7.54 (dd, *J*=7.9, 1.5, 1H, H8), 7.38 (td, *J*=7.7, 1.5, 1H, H10), 7.29 (td, *J*=7.7, 1.6, 1H, H9)	H7=Cl
6	10.00 (s, 1H)	3.84 (s, 3H)	7.01 (dd, *J*=8.1, 1.3, 1H)	6.86 (t, *J*=8.0, 1H)	7.51 (d, J=7.8, 1H)	8.55 (s, 1H),	11.94 (s, 1H)	9.33 (bs, 1H)	8.37 (d, *J*=7.7, 1H, H11), 7.23–7.14 (m, 1H, H9), 7.10 (dd, *J*=8.3, 1.3, 1H, H8), 6.97 (td, *J*=7.8, 1.3, 1H, H10)	H7=OCH_3: 3.89 (s, 3H)
7	10.11 (s, 1H)	3.83 (s, 3H).	7.00 (dd, *J*=8.0, 1.3, 1H).	6.81 (t, *J*=8.0, 1H),	7.71 (d, *J*=7.8, 1H),	8.55 (s, 1H)	11.93 (s, 1H)	9.30 (bs, 1H)	7.64 (dt, *J*=11.3, 2.2, 1H, H11), 7.47 (d, *J*=8.7, 1H, H7), 7.42-7.35 (m, 1H, H8), 7.03 (td, *J*=8.3, 2.5, 1H, H9)	H10=F
8	10.12 (s, 1H)	3.83 (s, 3H)	7.00 (dd, *J*=8.0, 1.3, 1H),	6.81 (t, *J*=8.0, 1H)	7.72 (d, *J*=7.9, 1H)	8.54 (s, 1H)	11.93 (s, 1H)	9.29 (bs, 1H)	7.78 (t, *J*=2.0, 1H, H11), 7.61 (dd, *J*=8.1, 1.0, 1H, H7), 7.39 (t, *J*=8.1, 1H, H8), 7.25 (ddd, *J*=8.0, 2.0, 0.8, 1H, H9)	H10=Cl
9	10.00 (s, 1H)	3.83 (s, 3H)	6.99 (dd, *J*=8.1, 1.4, 1H)	6.81 (t, *J*=8.0, 1H)	7.71 (d, *J*=7.8, 1H)	8.54 (s, 1H)	11.83 (s, 1H)	9.29 (bs, 1H)	7.32 (t, *J*=2.1, 1H, H11), 7.27 (t, *J*=8.0, 1H, H8), 7.22–7.18 (m, 1H, H7), 6.77 (ddd, *J*=8.1, 2.5, 1.0, 1H, H9),	H10=OCH_3: 3.77 (s, 3H)
10	9.89 (s, 1H)	9.86 (s, 1H)	6.40–6.28 (m, 1H)	6.40–6.28 (m, 1H)	7.67 (d, *J*=8.2, 1H)	8.38 (s, 1H)	11.71 (s, 1H)	9.92 (s, 1H)	8.39 (d, *J*=8.4, 1H, H11), 7.19–7.11 (m, 1H, H9), 7.09 (dd, *J*=8.2, 1.2, 1H, H8), 7.01 –6.87 (m, 1H, H10)	OCH_3: 3.88 (s, 3H)
11	9.79 (bs, 1H)	9.77 (s, 1H),	6.32 (d, *J*=2.3, 1H)	6.28 (dd, *J*=8.5, 2.2, 1H)	7.74 (d, *J*=8.6, 1H)	8.31 (s, 1H)	11.35 (s, 1H)	8.87 (t, *J*=6.1, 1H)	7.43–7.17 (m, 5H, benzyl, H7-H11)	CH_2: 4.83 (d, *J*=6.2, 2H

b)

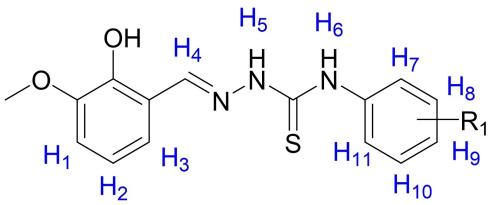

1-9

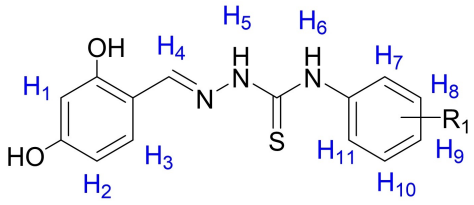

10-11

Comp. ID	OH	OCH_3/OH	H1	H2	H3	H4	H5	H6	H7-H11	R_1
1	6.25	4.31–3.93	7.14	7.04	7.51	8.49	8.86	7.18	7.94 (H7 = H11), 7.93 (H8 = H10), 7.91 (H9)	CH_2: 4.71
2	6.32	4.35–3.98	7.25	7.27	7.98	8.62	8.94	9.46	8.22 (H7), 7.68 (H8), 7.66 (H10), 7.32 (H11)	H9 = CH_3: 2.69–2.38
3	6.42	4.37–4.00	7.31	7.34	8.09	8.67	9.05	10.44	10.29 (H7), 8.88 (H8), 8.83 (H10), 7.54 (H11)	H9 = NO_2
4	6.37	4.36–4.00	7.27	7.31	8.07	8.65	8.95	10.44	10.18 (H7), 7.65 (H10), 7.61 (H8), 7.54 (H9)	H7 = F
5	6.38	4.35–3.99	7.26	7.28	8.10	8.65	8.97	10.74	10.43 (H7), 7.91 (H10), 7.73 (H8), 7.51 (H9)	H7 = Cl
6	6.36	4.36–4.00	7.26	7.34	8.14	8.62	8.89	10.73	10.10 (H7), 7.55 (H9), 7.37 (H8), 7.36 (H10)	H7 = OCH_3: 4.59–4.09
7	6.37	4.36–3.99	7.28	7.33	8.09	8.63	8.89	10.05	9.90 (H7), 7.79 (H8), 7.28 (H9), 7.23 (H11)	H10 = F
8	6.38	4.36–3.99	7.29	7.34	8.08	8.63	8.89	10.02	10.03 (H7), 7.75 (H8), 7.50 (H9 = H11)	H10 = Cl
9	6.38	4.36–3.95	7.27	7.32	8.10	8.62	8.86	10.04	9.55 (H7), 7.67 (H8), 7.10 (H9), 6.92 (H11)	H10 = OCH_3: 4.20-3.99
10	5.16	5.19	6.63	6.79	8.46	8.50	8.77	10.63	10.10 (H7), 7.55 (H9), 7.36 (H8), 7.34 (H10)	OCH_3: 4.57-4.08

Metabolic enzyme inhibition properties

The target thiosemicarbazones derivatives (**1-11**) were studied against the AChE and two pharmacologically relevant *h*CAs, the cytosolic *h*CA I and II. Enzyme inhibition constants (K_I) and are reported in Table 6 (see Supplementary Figure S25 for Lineweaver-Burk plots of compounds **4** and **1**).

i−) Novel thiosemicarbazones derivatives (**1**–**11**) inhibited strongly AChE with K_Is in the nanomolar range of 23.54 ± 4.34–185.90 ± 26.16 nM. In particular, 2-fluorophenyl analog (**4**) exhibited the best AChE inhibitory impact with K_I of 23.54 ± 4.34 nM followed by compounds **3** with K_I 31.23 ± 4.36 nM, and **1** with K_I 37.04 ± 4.72 nM. Regarding structure–activity relationships (SARs), derivatives **2**, **9**, and **10**, having a *p*-toly, 3-methoxyphenyl and -(2-methoxyphenyl)-2-(2,4-dihydroxybenzylidene moiety caused close effect on AChE inhibition. (**2**, K_I: 53.59 ± 7.98 nM; **9**, K_I: 52.33 ± 6.82 nM; **10**, K_I: 54.91 ± 7.39 nM). Regarding SARs, derivative **4** having a 2-fluorophenyl was found to be 2.77 times more effective than its chloro-substituted analog. The order of activity of fluorophenyl (**4**), chlorophenyl (**5**), and methoxyphenyl (**6**) at position 2nd of 2-(2-hydroxy-3-methoxybenzylidene)hydrazine-1-carbothioamide can be presented as **4** (K_I: 23.54 ± 4.34 nM) > **5** (K_I: 65.29 ± 9.36 nM) > **6** (K_I: 71.42 ± 9.03 nM). *N*-(3-chlorophenyl)-2-(2-hydroxy-3-methoxybenzylidene)hydrazine-1-carbothioamide (**8**) with K_I of 168.10 ± 21.76 nM, and *N*-benzyl-2-(2,4-dihydroxybenzylidene)hydrazine-1-carbothioamide (**11**) with K_I of 185.90 ± 26.16 nM showed lower activity towards AChE. Derivative **7** having a 3-fluorophenyl and derivative **9** having a 3-methoxyphenyl was found to be 2.25 and 3.31 times more effective than its 3-chlorophenyl substituted analog (**8**), respectively. All studied compounds showed better inhibition than the standard compound, THA (K_I: 320.20 ± 24.20 nM).

ii−) All of the synthesized thiosemicarbazones derivatives (**1-11**) potently inhibited the *h*CA I with K_I values in the range of 103.90 ± 23.49-325.90 ± 77.99 nM. The order of inhibition effects of these compounds against *h*CA I, K_I values can be presented as follows: **4** (K_I: 103.90 ± 23.49 nM) > **5** (K_I: 122.60 ± 23.36 nM) > **6** (K_I: 125.00 ± 19.46 nM) > **9** (K_I: 158.60 ± 36.60 nM) > **1** (K_I: 173.30 ± 33.67 nM) = **10** (K_I: 173.60 ± 33.58 nM) > **3** (K_I: 190.80 ± 35.71 nM) > **8** (K_I: 191.90 ± 39.37 nM) > **11** (K_I: 243.50 ± 41.92 nM) > **2** (K_I: 249.00 ± 53.51 nM) > **7** (K_I: 325.90 ± 77.99 nM). The order of activity of fluorophenyl (**4**), chlorophenyl (**5**), and methoxyphenyl (**6**) at position 2nd of 2-(2-hydroxy-3-methoxybenzylidene)hydrazine-1-carbothioamide can be presented as **4** > **5** > **6**. This situation is similar to AChE. The order of activity of fluorophenyl (**7**), chlorophenyl (**8**), and methoxyphenyl (**9**) at position 3rd of 2-(2-hydroxy-3-meth-

Table 5. a) Experimental ^{13}C-NMR data of the compounds, (δ/ppm). b) Calculated ^{13}C-NMR data of the compounds, (ppm).

a)

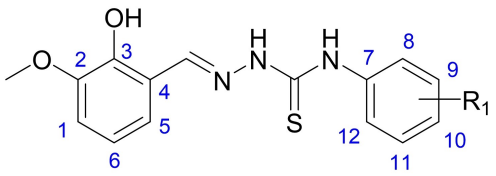

1-9

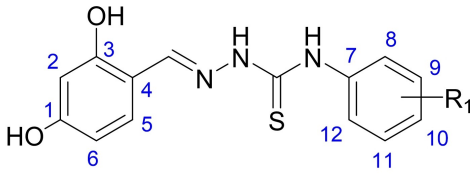

10-11

Comp. ID	OCH_3	C1	C2	C3	C4	C5	C6	CH=N	C=S	ArC7-C12	R_1
1	55.90	112.86	146.00	147.95	118.92	120.83	118.20	139.46	177.43	139.53, 128.13, 127.23, 126.68 (benzyl C7-C12)	CH_2: 46.60
2	55.92	113.04	146.16	147.92	118.93	120.71	118.53	139.89	175.82	136.57 (C10), 134.30 (C7), 128.47 (C9, C11, C9=C11), 125.58 (C8, C12, C8=C12),	CH_3: 20.56
3	55.93	113.38	146.49	147.96	118.98	120.38	118.50	141.16	175.05	145.51 C7), 143.33 (C10), 124.16 (C8, C12, C8=C12), 123.69 (C9, C11, C9=C11)	C10=NO_2
4	55.92	113.09	146.24	147.96	118.96	120.66	118.27	140.06	176.94	157.15 (d, *J*=246.5, C8), 129.90 (s, C11) 127.88 (d, *J*=7.8, C10), 127.25 (d, *J*=11.8, C7), 123.91 (d, *J*=3.5, C12), 115.58 (d, *J*=20.0, C9)	C8=F
5	55.93	113.13	146.31	147.99	119.06	120.61	118.05	140.03	176.18	136.47 (C7), 129.94 (C9), 129.23 (C8), 129.11 (C11), 127.43 (C10), 127.06 (C12)	C8=Cl
6	55.93	113.11	146.37	148.12	119.26	120.64	117.29	139.40	174.54	150.92 (C8), 127.86 (C7), 125.33 (C10), 123.08 (C12), 119.87 (C11), 111.17 (C9)	C8=OCH_3: 56.00
7	55.92	113.19	146.31	147.94	118.95	120.55	118.52	140.45	175.46	161.50 (d, *J*=241.6, C9), 140.90 (d, *J*=10.9, C7), 129.42 (d, *J*=9.3, C11), 121.04 (s, C12), 111.95 (d, *J*=24.7,C8), 111.53 (d, *J*=20.9, C10)	C9=F
8	55.93	113.19	146.31	147.93	118.94	120.56	118.52	140.45	175.55	140.65 (C7), 132.11 (C9), 129.51 (C11), 124.91 C10), 124.77 C8), 123.94 (C12)	C9=Cl
9	55.92	113.11	146.24	147.93	118.97	120.64	118.54	140.11	175.48	159.01 (C11), 140.23 (C7), 128.71 (C9), 117.49 (C10), 110.99 (C8), 110.60 (C12)	C11=OCH_3: 55.14
10	–	158.36	102.42	160.83	127.97	111.66	108.10	140.54	173.88	150.71 (C8), 127.42 (C7), 125.05 (C10), 122.81 (C12), 119.83 (C11), 111.12 (C9)	C8=OCH_3: 56.00
11	–	157.98	102.33	160.47	128.35	111.85	107.71	140.69	176.92	139.67, 128.11, 127.22, 126.65 (benzyl C7–C12)	CH_2: 46.54

b)

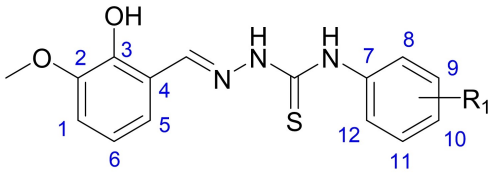

1-9

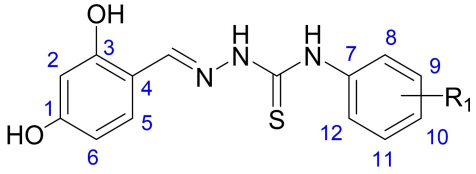

10-11

Comp. ID	OCH_3	C1	C2	C3	C4	C5	C6	CH=N	C=S	ArC7-C12	R_1
1	57.90	115.88	154.51	154.26	124.82	120.75	124.99	142.64	184.03	143.92 (C7), 136.65 (C8=C12), 134.95 (C9=C11), 134.57 (C10)	CH_2: 54.11

2	57.97	116.33	154.48	154.66	124.79	121.05	125.25	143.44	183.81	145.07 (C10), 147.44 (C7), 135.08 (C11), 134.14 (C9), 132.51 (C8), 129.01 (C12)	CH_3: 22.49
3	58.03	117.02	154.44	155.08	124.17	121.35	125.43	144.59	181.97	153.78 (C7), 149.62 (C10), 132.77 (C9), 132.09 (C11), 125.63 (C12), 121.30 (C8)	C10 = NO_2
4	58.01	116.53	154.40	154.79	124.54	121.19	125.38	143.58	180.86	162.25 (C12), 134.91 (C7), 129.81 (C9), 129.58 (C10), 123.41 (C8), 120.22 (C11)	C8 = F
5	57.99	116.64	154.35	154.78	124.49	121.30	125.35	143.84	181.26	143.22 (C7), 136.47 (C12), 135.48 (C11), 133.07 (C9), 129.96 (C10), 123.69 (C8)	C8 = Cl
6	57.97	116.32	154.37	154.54	124.80	121.13	125.38	142.95	180.41	156.32 (C12), 135.25 (C7), 129.72 (C10), 124.44 (C9), 121.98 (C8), 113.79 (C11)	C8 = OCH_3: 57.68
7	57.99	116.58	154.42	154.81	124.51	121.14	125.42	143.48	181.16	173.20 (C11), 148.41 (C7), 136.50 (C9), 117.85 (C8), 115.78 (C10), 111.39 (C12)	C9 = F
8	57.99	116.60	154.41	154.75	124.50	121.19	125.38	143.47	181.16	148.18 (C11), 148.11 (C7), 136.09 (C9), 129.48 (C10), 124.92 (C12), 120.15 (C8)	C9 = Cl
9	57.97	116.42	154.41	154.65	124.64	121.11	125.36	143.03	180.92	168.49 (C11), 148.03 (C7), 135.34 (C9), 118.20 (C10), 113.18 (C8), 105.65 (C12)	C11 = OCH_3: 57.07
10	-	168.63	105.35	166.23	118.26	133.32	112.69	143.23	179.93	156.22 (C12), 135.34 (C7), 129.33 (C10), 124.32 (C9), 121.79 (C9), 113.67 (C11)	C8 = OCH_3: 57.63

oxybenzylidene)hydrazine-1-carbothioamide can be presented as **9** > **8** > **7**. When the inhibition values are examined, *N*-benzyl-2-(2-hydroxy-3-methoxybenzylidene)hydrazine-1-carbothioamide (**1**) and *N*-benzyl-2-(2,4-dihydroxybenzylidene)hydrazine-1-carbothioamide (**11**) groups did not cause any change in inhibition. When the benzyl, *p*-tolyl and 4-nitrophenyl bonded compounds are compared among themselves, the inhibition order is as follows: benzyl (**1**) > 4-nitrophenyl (**3**) > *p*-tolyl (**2**). All studied compounds showed better inhibition than the standard compound, AAZ (K_I: 422.00 ± 5.53 nM).

iii−) The thiosemicarbazones derivatives (**1**–**11**) showed potent inhibition effect on *h*CA II enzyme activity with K_I values range of 86.15 ± 18.58-287.70 ± 43.09 nM. *N*-benzyl analog (**1**) exhibited the best *h*CA II inhibitory impact with K_I of 86.15 ± 18.58 nM followed by 2-chlorophenyl analog (**5**) with K_I 98.45. ± 19.75 nM. When the benzyl, *p*-tolyl and 4-nitrophenyl bonded compounds are compared among themselves, the inhibition order is as follows: benzyl (**1**) > *p*-tolyl (**2**) > 4-nitrophenyl (**3**). Regarding SARs, the order of activity of 2-methoxyphenyl, 2-fluorophenyl, and 2-chlorophenyl can be presented as 2-chlorophenyl (**5**, K_I: 98.45 ± 19.75 nM) > 2-fluorophenyl (**4**, K_I: 247.80 ± 39.81 nM) > 2-methoxyphenyl (**6**, K_I: 273.20 ± 32.25 nM). Derivative **5** was found to be 2.78 times more effective than its substituted methoxy analog. In addition to, the order of activity of 3-methoxyphenyl, 3-fluorophenyl, and 3-chlorophenyl can be presented as 3-fluorophenyl (**7**, K_I: 120.10 ± 30.07 nM) > 3-methoxyphenyl (**9**, K_I: 155.60 ± 19.75 nM) > 3-chlorophenyl (**8**, K_I: 287.70 ± 43.09 nM). Except for compounds **3**, **4**, **6**, **8** other studied compounds showed better inhibition than the standard compound, AAZ (K_I: 226.60 ± 6.96 nM).

Numerous thiosemicarbazones derivatives have been studied to find potent and AChE and selective *h*CAs inhibitors. In our team's previous work, novel thiosemicarbazone derivatives were created and produced via Schiff base condensation processes involving various substituted thiosemicarbazides. These compounds exhibited highly potent inhibition AChE and *h*CAs.[31] In our other work, by combining different isocyanates with 4-hydroxy-3,5-dimethoxy benzaldehyde, new thiosemicarbazones carrying the Schiff base (**1**–**13**) were produced. The compounds showed highly potent inhibition effect with K_I values are in the range of 51.11–78.10 nM for AChE, 60.32–300.00 nM for *h*CA I, and 64.21–307.70 nM, for *h*CA II.[32] Hasmi et al.[38] developed, described, and tested the biological activity of a new class of 4-(Diethylamino)salicylaldehyde based thiosemicarbazones against CAs enzymes. They discovered that these substances chemicals inhibited the *h*CA I isoform, with K_I values between 407.73 and 1104.1 nM. For *h*CA II, K_Is range from 323.04-991.62 nM. Eraslan-Elma and colleagues[39] created 1*H*-indole-2,3-dione 3-thiosemicarbazones and investigated how to block *h*CA I, II, IX, and XII enzymes. They demonstrated that compared to other isoenzymes, hCA II isoenzyme was more inhibited by produced drugs with nanomolar values (K_I ranged between 0.32 and 83.3 nM). 1*H*-indole-2,3-dione 3-thiosemicarbazones demonstrated a better inhibitory effect

Table 6. Inhibition data of *h*CAs and AChE with novel thiosemicarbazones (**1**–**11**) and standard drugs AAZ and THA.

Compound ID	AChE			*h*CA I			*h*CA II		
	K_I (nM)	R^2	Inhibition type	K_I (nM)	R^2	Inhibition type	K_I (nM)	R^2	Inhibition type
1	37.04 ± 4.72	0.9750	Competitive	173.30 ± 33.67	0.9481	Competitive	86.15 ± 18.58	0.9336	Competitive
2	53.59 ± 7.98	0.9684	Competitive	249.00 ± 53.51	0.9411	Competitive	209.00 ± 49.59	0.9327	Competitive
3	31.23 ± 4.36	0.9678	Competitive	190.80 ± 35.71	0.9653	Competitive	279.50 ± 49.49	0.9279	Noncompetitive
4	23.54 ± 4.34	0.9443	Competitive	103.90 ± 23.49	0.9294	Competitive	247.80 ± 39.81	0.9399	Noncompetitive
5	65.29 ± 9.36	0.9621	Competitive	122.60 ± 23.36	0.9484	Competitive	98.45 ± 19.75	0.9472	Competitive
6	71.42 ± 9.03	0.9718	Competitive	125.00 ± 19.46	0.9643	Competitive	273.20 ± 32.25	0.9469	Noncompetitive
7	74.79 ± 11.89	0.9541	Competitive	325.90 ± 77.99	0.9423	Competitive	120.10 ± 30.07	0.9265	Competitive
8	168.10 ± 21.76	0.9726	Competitive	191.90 ± 39.37	0.9447	Competitive	287.70 ± 43.09	0.9098	Noncompetitive
9	52.33 ± 6.82	0.9733	Competitive	158.60 ± 36.60	0.9244	Competitive	155.60 ± 19.75	0.9123	Noncompetitive
10	54.91 ± 7.39	0.9673	Competitive	173.60 ± 33.58	0.9576	Competitive	132.60 ± 16.06	0.9283	Noncompetitive
11	185.90 ± 26.16	0.9670	Competitive	243.50 ± 41.92	0.9616	Competitive	142.30 ± 26.65	0.9528	Competitive
THA [a]	320.20 ± 24.20	0.9927	Competitive	–	–	–	–	–	–
AAZ [b]	–	–	–	422.00 ± 5.53	0.9994	Noncompetitive	226.60 ± 6.96	0.9974	Noncompetitive

[a] Tacrine. [b] Acetazolamide.

when compared to our findings. Yakan et al.[3] created thiosemicarbazone compounds and researched the inhibition of the AChE enzyme. The compounds had a strong AChE inhibitory action, and their K_I values ranged from 1.93 to 12.36 nM. These compounds showed stronger inhibitory efficacy as compared to our findings. The many groups that are connected to the thiosemicarbazone structure may be to blame for this.

DFT analysis

The electronic properties of compounds are affected by their conformation, and due to the effects of both electrostatic interactions and steric effects on the conformations during a reaction, it is expected that there will be some discrepancies between the electronic data obtained from isolated single-state DFT calculations and the experimental results. However, some electronic reactivity parameters of the compounds can provide some useful estimates in comparing the reaction properties of the compounds relative to each other.

Considering the substituted structures and structural similarities, the compounds synthesized within the scope of this study can be examined in two groups in general: the first group is methyl, methoxy, NO_2, F, and Cl substituted compounds **2**–**9**; the second group of compounds can be classified as **1**, **10**, and **11**. In all compounds, it was observed that HOMOs and LUMOs were generally distributed (except methoxy substituted compounds) in the phenolic imine region, while *p*-methyl substituted compound **2** and *o*-, *m*-methoxy substituted compounds **6** and **9** also showed that HOMOs were also distributed over the aniline region. ESP-HOMO and LUMO maps of compounds **6** and **10** are provided in Figure 1 for ease of comparison (see Supplementary Figure S23 for all ESP-HOMO, and LUMO maps). *m*-Substituents contribute to inductive effects, while *para* substituents contribute to both inductive and resonant effects. Since the electron-donating resonance effect dominate the electron-withdrawing inductive effect, the methoxy substituent acts as an electron-withdrawing at the *meta* position while acting as an electron donating group at the *para* position. Electron-donating groups enrich a nucleophilic site with electrons and increase the compound's tendency to attack electrophilic sites, i.e., making nucleophiles stronger. Electron-withdrawing groups, on the other hand, are those that reduce the electron density in a site through the carbon atom to which they are attached, making electrophiles stronger, or, conversely, making any nucleophilic species less reactive. It was observed that electron-withdrawing fluorine, chlorine, and NO_2 substituents can affect the distribution of HOMOs on the phenyl ring at a much lower level than the electron-donating groups such as methyl and methoxy.

Although the electronic parameters given in Table 7 provide partial information about the activities of the compounds, it is difficult to precisely determine the parameters related to the activities of the compounds when the compound groups are examined comparatively among themselves. For example, values for compounds **7**–**9**, a correlation can be established between E_{HOMO}, E_{LUMO}, electrophilic index, electroaccepting-

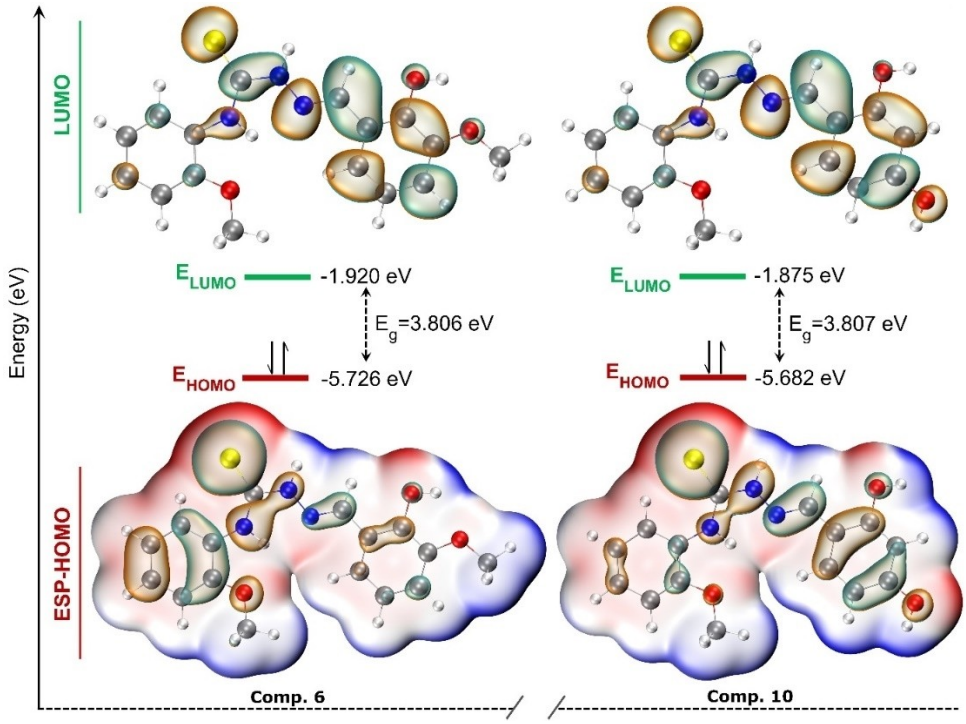

Figure 1. ESP-HOMO and LUMO surface of the compounds **6** and **10** (Energy gap $E_g = E_{LUMO} - E_{HOMO}$).

Table 7. Quantum chemical parameters of the compounds obtained from DFT calculations.

Comp.	E_{HOMO} (eV)	E_{LUMO} (eV)	E_g (eV)	η (eV)	χ (eV)	ω (eV)	**ε**(eV)	***μ*** *Debye*	ω^+ (eV)	ω^- (eV)
1	−5.712	−1.842	3.870	1.935	3.777	3.686	3.783	8.105	0.438	4.215
2	−5.809	−1.985	3.824	1.912	3.897	3.971	3.686	7.972	0.515	4.412
3	−6.252	−2.687	3.565	1.783	4.470	5.603	3.243	12.91	1.013	5.482
4	−5.919	−2.028	3.891	1.946	3.974	4.058	3.576	7.025	0.528	4.502
5	−5.930	−2.040	3.890	1.945	3.985	4.082	3.565	6.833	0.535	4.520
6	−5.726	−1.920	3.806	1.903	3.823	3.840	3.769	8.838	0.484	4.307
7	−5.982	−2.112	3.870	1.935	4.047	4.232	3.513	7.858	0.576	4.623
8	−5.999	−2.124	3.875	1.938	4.062	4.257	3.496	7.853	0.582	4.644
9	-5.862	-2.034	3.828	1.914	3.948	4.072	3.633	9.398	0.540	4.488
10	−5.682	−1.875	3.807	1.904	3.779	3.750	3.813	7.679	0.462	4.240
11	−5.661	−1.840	3.821	1.911	3.751	3.681	3.834	6.874	0.443	4.194

E_{HOMO}: HOMO Energy, E_{LUMO}: LUMO Energy, E_g: $E_{LUMO} - E_{HOMO}$, η: Chemical Hardness, χ : Electronegativity, ω: Electrophilic index, **ε**: Nucleophilic index, ***μ***: Dipole moment, ω^+: Electroaccepting power, ω^-: Electrodonating power.

electrodonating power values and AChE enzyme inhibition, but since substituents change the electron distributions and electronic parameters of the compounds through intramolecular interactions, making generalizations based on the electronic data of compounds referring to enzyme inhibitory activity may lead to misinterpretation of existing results. However, within the scope of this study, some analyses were carried out by taking into account the effects of substituted groups on the compounds.

We can say that FMOs are among the factors affecting the chemical stability and reactivity of the drug molecule in the studies of structure–activity relationships. While HOMOs mostly play an active role as electron donors, LUMOs accepts electrons. Moreover, the smaller the HOMO-LUMO energy gap (E_g), the easier it is to break the reactant bonds and, accordingly, the greater the tendency for product bonds to form. The smaller the E_g, the greater the tendency for reactant bonds to break and product bonds to form. In this context, compounds **2**, **3**, **6**, and **9**–**11** are expected to be more reactive than other compounds, but it should be noted that E_g alone is not a parameter that can determine reactivity. Also, the higher energy of HOMO is associated with stronger nucleophilicity of the

compound, while the lower energy of LUMO corresponds to more electrophilic behavior. In this respect, it can be said that compounds **2**, **6**, and **9**–**11** with low E_g are more nucleophilic ($E_{HOMO} > -5.862$ eV) than other compounds ($E_{HOMO} < -5.919$ eV), except for compound **1** and NO_2 substituted compound **3** (see Table 7). In this context, it can be assumed that *h*CA I enzyme inhibitions of *o*-chlorine and *m*-fluorine/chlorine substituted compounds **5** and **7**, **8**, respectively, occur through dominant nucleophilic attacks. Because while the expectation of electrophilic properties depending on LUMO energy of these compounds increases, it is seen that *h*CA I enzyme inhibitions are generally low. On the other hand, it has been observed that fluorine and chlorine substituents do not have similar effects in all enzyme inhibition reactions. In *h*CA II enzyme inhibitions, while *o*-fluorine and chlorine are the dominant nucleophilic attack inhibitors, more dominant electrophilic attack reactions can be predicted for *meta* positions. In AChE enzyme inhibition, the data support the expectation of nucleophilic attack in the *ortho* position and more dominant electrophilic attack in the *meta* position of fluorine. For compounds **6** and **9**, it can also be said that the *meta* position of methoxy, relative to the *ortho* position, refers *h*CA I and AChE inhibitions to electrophilic attack, while *h*CA II inhibition refers to nucleophilic attack. In addition, the *ortho* position of the methoxy substituent had a negative effect on the inhibition reactions compared to *o*-fluorine and *o*-chloro, while its *meta* position contributed positively to the inhibition. At this point, although the dependence of the electron density of the phenyl ring on the *ortho* and *meta* positions of the electronegative atoms can be considered as a result of inductive and resonance effects, the available data are not sufficient to reach definite conclusions.

The interatomic/intramolecular interactions of the compounds and the electron densities of these interactions can be examined in more detail with QTAIM calculations and IRI maps (see Figure 2 for compound **2**; all data is given in Supplementary Figures S24a–c).

In addition to the strong intramolecular interactions of S···Phenyl-R, –NH···N, and OH···OCH_3, the intramolecular interactions of *ortho* substituents with neighbouring –NH cause local electron delocalization on those regions of the compounds. For this case, the fact that the electrons delocalized due to intramolecular interactions can move more freely in the interaction region may lead to the assumption that they cause the compounds to increase enzyme inhibition, or it can be considered that delocalization causes compounds to be more favorable for nucleophilic attacks due to the fact that it reduces the electron density outside the intramolecular interaction region. This assumption is supported by that *o*-F, *o*-Cl and *o*-methoxy substituted compounds **4**–**6**, where the substituents show strong intramolecular interactions, show a higher *h*CA I/*h*CA II inhibition effect than *m*-F, *m*-Cl and *m*-methoxy-substituted compounds **7**–**9**. In addition, for AChE and *h*CA I inhibitions, the weaker inhibition effect of electron-donating CH_3 substituted compound **2** than electron-withdrawing NO_2 substituted compound **3** leads to the opinion that the compounds are exposed to nucleophilic attacks through the phenol structure to which they are attached. In this respect, compound **4**, to which the fluorine atom is attached, which is more electronegative than chlorine, is expected to be more reactive than compound **5**, and experimental results confirmed this expectation (see Table 6). Moreover, the fact that electron donor *o*-MeO substituted compound **6** has a weaker inhibition effect than electron withdrawing substituted compounds **4** and **5** strengthens this assumption. A similar situation was observed for compounds **10** and **11**: Compound **10** has a lower electron density in the RCP on the non-substituted phenyl ring than compound **11** (0.022527 *e*/bohr^3 for compound **10**; 0.023239 *e*/bohr^3 for compound **11**), but compound **10** showed a higher inhibition effect (see Supplementary Figure S23). In general, for the enzyme inhibition properties of the compounds on *h*CA I and *h*CA II, it can be said that compounds with electron withdrawing substituents in the *para* position are more active

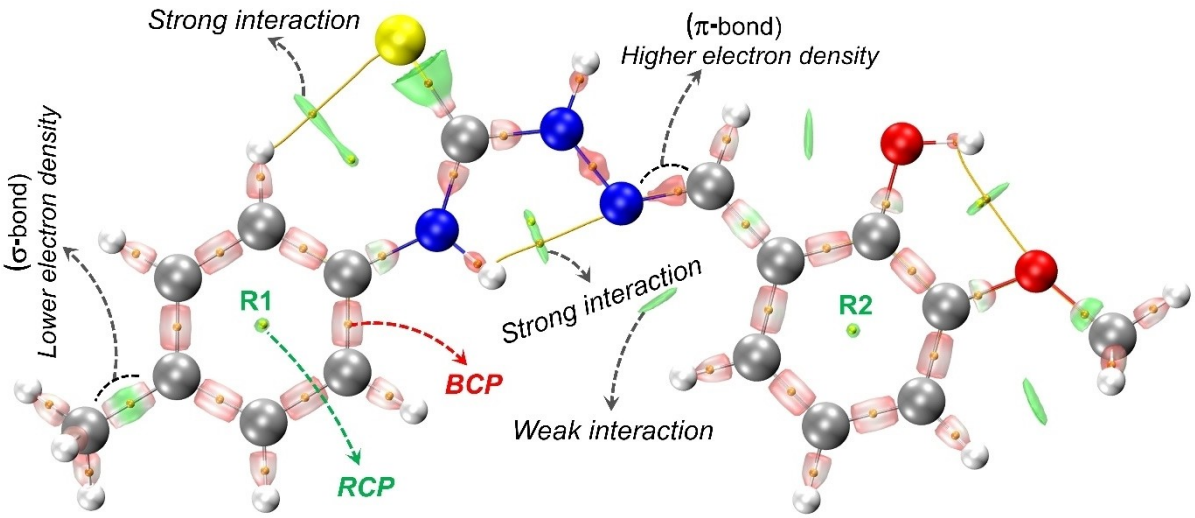

Figure 2. IRI surface of intramolecular interaction and QTAIM critical points (*e*/bohr^3) of compound **2** (RCP: Ring Critical Point, BCP: Bond Critical Point).

than compounds with identical substituents at the *meta* position.

Data were also obtained supporting a prediction that inhibition reactions of *meta*-substituted compounds occur via electrophilic attacks, *m*-methoxy, for example, has a higher electron-withdrawing effect than *m*-Cl, and this indicates that compound **9** is capable of stronger electrophilic attacks than compound **8** through the regions to which the substituents are attached. A similar situation is observed for compounds **7** and **8**. The fluorine (or chlorine) atom has both inductively electron withdrawing and mesomerically electron donor properties, and while the inductive effect is identical for the *para* and *meta* positions, the mesomeric effect dominates at the *para* and *ortho* position. Fluorine atom is more electronegative than chlorine and has a higher inductive effect, and as a result, compound **7** may have shown higher enzyme inhibition than compound **8** via electrophilic attacks on AChE and *h*CA II. At this point, it should not be overlooked that although some consistent approximations can be made with the electronic data obtained as a result of the calculations, enzyme inhibition reactions are more complex and depend on more variables. Much more studies are needed to see the relevant correlations and understand their properties.

Molecular docking calculations

A comprehensive study was conducted to investigate the binding modes of novel synthesized thiosemicarbazones bearing Schiff-bases (**1**–**11**) within the THA and AAZ binding sites of AChE and *h*CAs, respectively. The performance of the Glide XP docking protocol was evaluated by re-docking the co-crystallized THA and AAZ into the active sites of AChE (PDB ID 7XN1) and *h*CAs (PDB IDs 1AZM and 3HS4 for *h*CA I and II, respectively), and using Schrödinger Small-Molecule Drug Discovery Suite 2023-1 for Mac (Schrödinger, LLC). The RMSD values between the native ligands, THA, and AAZ conformation and the best pose generated by this protocol were 0.27, 0.37, and 1.04 Å, respectively. These values indicate that the Glide XP docking algorithm was deemed qualified for docking thiosemicarbazones (**1**–**11**) to the active pockets of AChE and *h*CAs.

The competitive inhibitors **4** (K_Is of 23.54 ± 4.34 nM and 103.90 ± 23.49 nM for AChE and *h*CA I, respectively) and **1** (K_I of 86.15 ± 18.58 nM for *h*CA II) have established primary contacts through hydrogen bonding and π-π stacking (excluding compound **1**). These inhibitors have docking scores of −9.883, −5.661, and −5.230 kcal/mol with 7XN1, 1AZM, and 3HS4, respectively. The potent inhibitor **4** has formed hydrogen bonds with Asp74, Trp86 (water-mediated), and Tyr337 at distances of 2.31, 2.02, and 2.18 Å, respectively. In addition, it has formed π-π stacking interactions with Trp86 and Tyr337, and hydrophobic interactions with residues Tyr124, Trp286, Val294, Phe295, Phe297, Phe338, Tyr341, Trp439, and Tyr449 (Figure 3). The most active compound against *h*CA I, **4**, has displayed H-bonds with Gln92 (water-mediated) and water molecules at distances of 1.96 and 2.23 Å, respectively. Furthermore, it has formed π-π stacking interaction with His67, and hydrophobic interactions with Ile60, Val62, Phe91, Ala121, Leu131, Ala135, Leu141, Val143, Leu198, and Trp209, as depicted in Figure 4. Compound **1** has shown H-bonds with Gln92 and two water molecules at the distances of 2.57, 1.78, and 2.73 Å, respectively, along with hydrophobic interactions with Ile91, Val121, Phe131, Leu141, Val143, Leu198, Val207, and Trp209, as shown in Figure 5. The inhibitors' docking scores and binding poses have proven their potency as competitive inhibitors against AChE and *h*CAs.

Furthermore, the potential of the synthesized thiosemicarbazones with Schiff-bases (**1**–**11**) to serve as drugs were evaluated by analyzing their descriptor scores and ADME-related parameters, which were calculated utilizing the Schrodinger QikProp module of the Schrödinger Suite 2023-1 for Mac. The results indicated that all compounds (**1**–**11**) adhered to both Lipinski's five[40] and Jorgensen's three[41] rules, suggesting their potential as viable drug candidates (Table 8). These findings highlight the potential of thiosemicarbazones bearing Schiff bases as promising drug molecules with favorable pharmacological properties.

Conclusions

The eleven novel thiosemicarbazone hybrid skeletons were designed and synthesized by the condensation of two different aldehyde derivatives with various substituted-thiosemicarbazides, and isolated in good yields with 68–95 %. The structures of all compounds have been characterized by FT-IR, ^{1}H, and ^{13}C-NMR spectroscopy, and elemental analysis. The structural and spectroscopic characterization of these new compounds were found to be in decent agreement with both theoretical (DFT calculations) and experimental data. In addition to the substituent groups affecting enzyme inhibition differently depending on their structure, it has been revealed by DFT calculations that intramolecular interactions also have an effect on electron delocalization and enzyme inhibition. The compounds with electron-withdrawing substituents, especially at the *para* position, tended to be more reactive in enzyme inhibition. The *meta*-substituted compounds were predicted to undergo electrophilic attack. The electron-withdrawing effect of *m*-methoxy indicated stronger electrophilic attacks compared to *m*-Cl. As a result of DFT calculations, some findings were found that there may be a correlation, albeit rough, between the FMO energy eigenvalues of the compounds and their inhibition reactivities. Examining this correlation revealed some data on the usability of QTAIM and IRI calculations to more accurately interpret the dependence of the electrophilic or nucleophilic attacks of compounds on the positions of the substituents. Both *in vitro* and molecular docking investigations have confirmed the inhibitory activities of recently synthesized thiosemicarbazones containing Schiff-bases (**1**–**11**) against AChE and *h*CAs and have revealed that the reference drugs THA and AAZ, along with these compounds, can bind into the same pocket. These thiosemicarbazones have demonstrated significant usefulness in their ADME characteristics, making them potential candidates for drug development. The findings of this research highlight

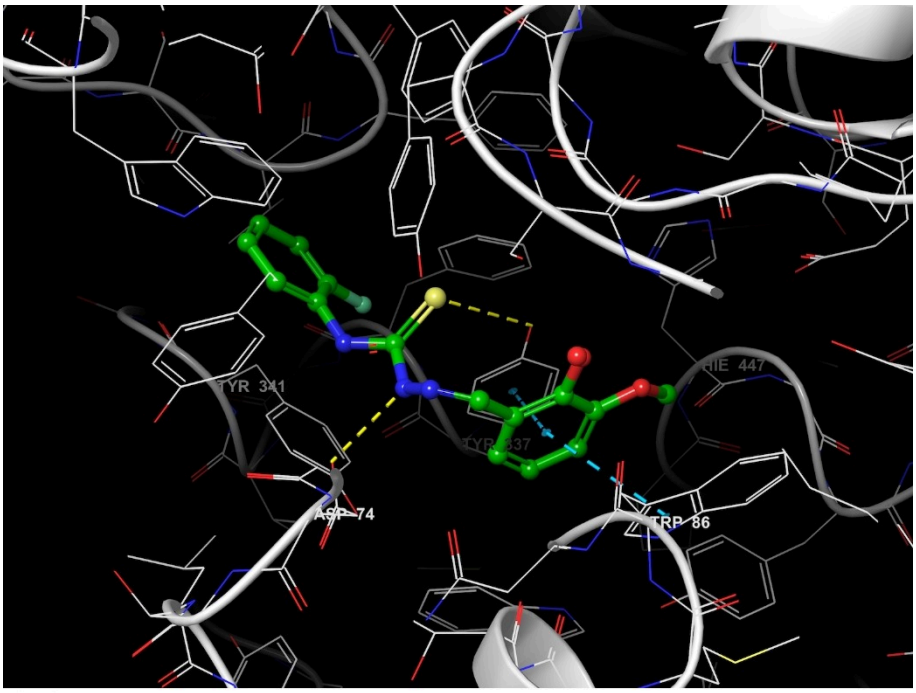

(a)

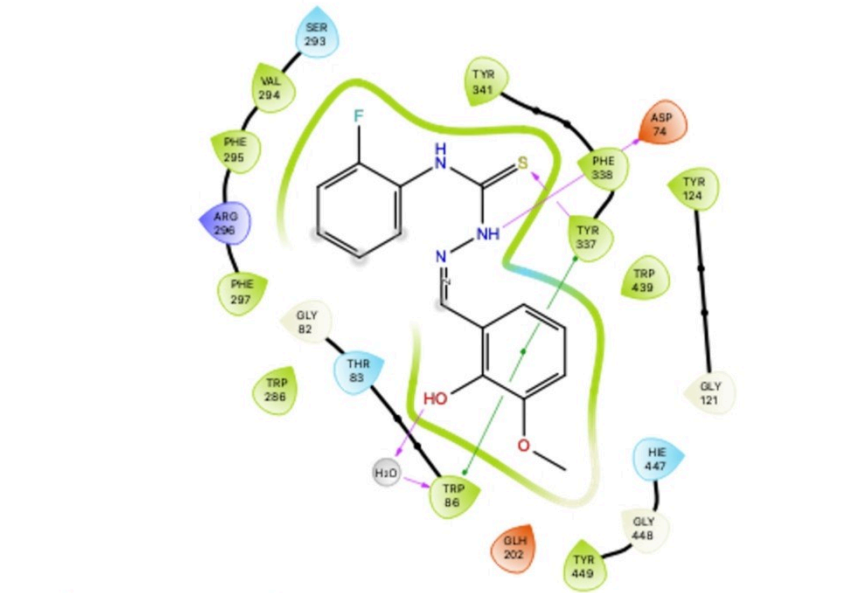

(b)

Figure 3. (**a**) 3D interaction of the compound **4** (*N*-(2-fluorophenyl)-2-(2-hydroxy-3-methoxybenzylidene)hydrazine-1-carbothioamide) with the key amino acids within the active site of AChE (PDB ID 7XN1). (**b**) 2D docking pose of the compound **4** (*N*-(2-fluorophenyl)-2-(2-hydroxy-3-methoxybenzylidene)hydrazine-1-carbothioamide) with the key amino acids within the binding site of AChE (PDB ID 7XN1).

the potential of thiosemicarbazones in developing new drugs for treating AD and other illnesses.

Experimental Section

Measurement and reagents

The detailed knowledge is given in Supporting Materials.

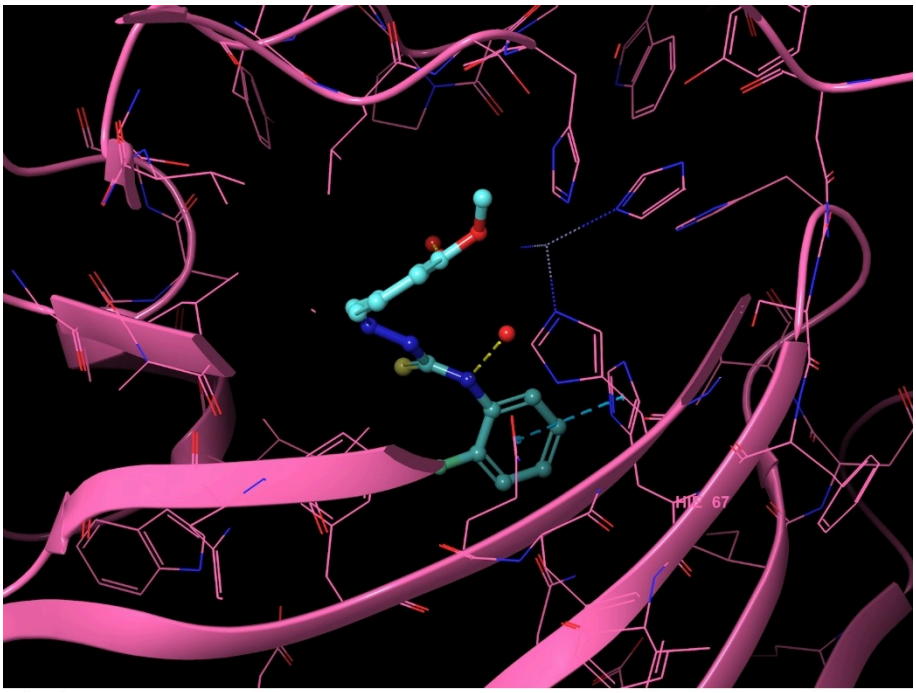

(a)

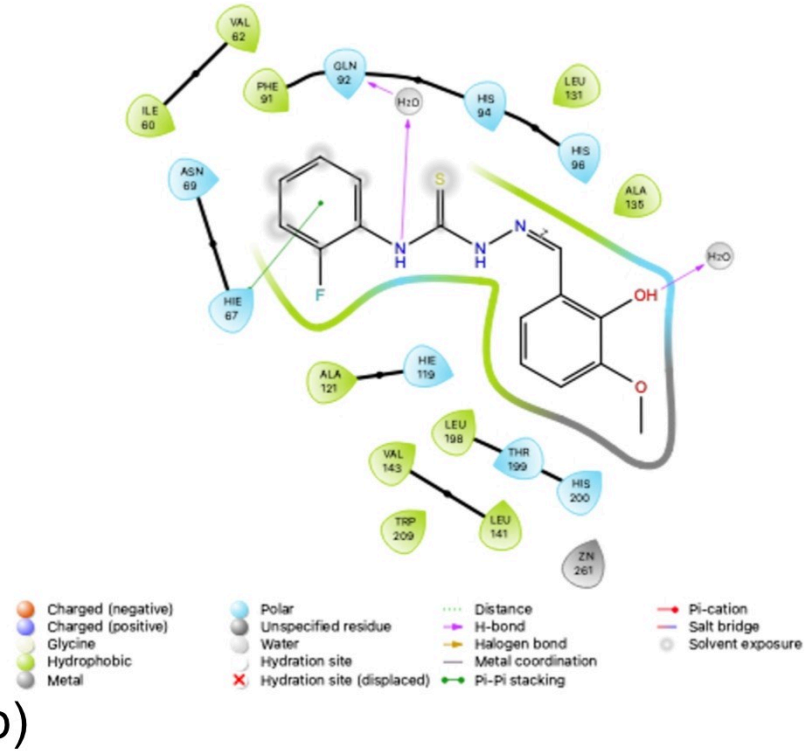

(b)

Figure 4. (**a**) 3D interaction of the compound **4** (*N*-(2-fluorophenyl)-2-(2-hydroxy-3-methoxybenzylidene)hydrazine-1-carbothioamide) with the key amino acids within the active site of *h*CA I (PDB ID 1AZM). (**b**) 2D docking pose of the compound **4** (*N*-(2-fluorophenyl)-2-(2-hydroxy-3-methoxybenzylidene)hydrazine-1-carbothioamide) with the key amino acids within the binding site of *h*CA I (PDB ID 1AZM).

Synthesis of thiosemicarbazone derivatives (1–11)

Various isothiocyanate (8.00 mmol) derivatives in (15 mL) ethanol are added dropwise to the solution of hydrazine monohydrate (8.00 mmol) in (25 mL) ethanol cooled in an ice bath, with vigorous stirring. The reaction mixture was kept in a refrigerator overnight. The resulting precipitate was filtered, dried, and purified with ethanol to afford thiosemicarbazides. Then, the formed thiosemicarbazides (4.00 mmol), 3-methoxy or 4-hydroxysalicylicaldehyde

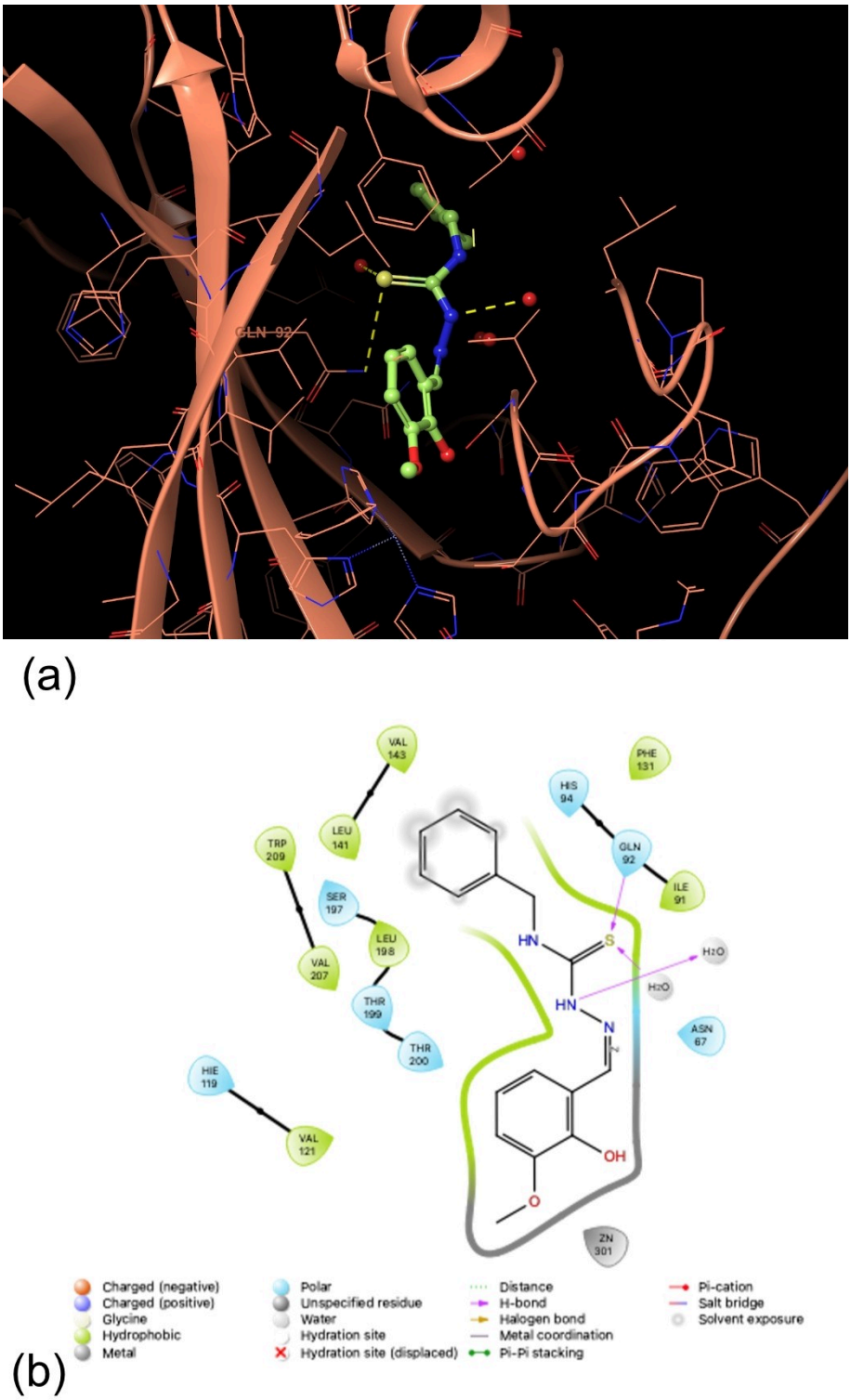

Figure 5. (**a**) 3D interaction of the compound **1** (*N*-benzyl-2-(2-hydroxy-3-methoxybenzylidene)hydrazine-1-carbothioamide) with the key amino acids within the active site of *h*CA II (PDB ID 3HS4). (**b**) 2D docking pose of the compound **1** (*N*-benzyl-2-(2-hydroxy-3-methoxybenzylidene)hydrazine-1-carbothioamide) with the key amino acids within the binding site of *h*CA II (PDB ID 3HS4).

(4.00 mmol), and one drop of HCl were added to aqueous ethanol (25 mL) and the mixture was refluxed at 78 °C for 3–5 h. The crude product was filtered, washed with ethanol, and dried in air. The compounds were successfully prepared with good yields (68–95 %) as shown in Scheme 2. These new compounds were synthesized according to the procedure described in the literature.[42]

Table 8. ADME-related parameters [a] of the targeted novel synthesized thiosemicarbazones bearing Schiff-bases (1–11) and clinically used reference inhibitors tacrine and acetazolamide.

Compound ID	#stars	#rtvFG	CNS	MW	Dipole	SASA	Volume	donorHB	accptHB	QPlogPC16	QPlogPoct	QPlogPw	QPlogPo/w	QPlogS	QPPCaco	QPlogBB	QPPMDCK	QPlogKp	#metab	QPlogKhsa	HOA	PSA	Rule of Five	Rule of Three
1	1	0	−1	315.4	12.9	665.8	1035.7	3.0	5.5	11.6	20.5	12.1	3.1	−4.3	1403	−0.6	1413	−1.4	3	−0.02	100	71.4	0	0
2	1	0	−1	315.4	13.3	619.4	1044.0	3.0	5.5	11.5	20.8	12.1	3.1	−4.7	1416	−0.6	1527	−1.6	3	0.04	100	70.8	0	0
3	1	0	−2	346.4	16.4	625.8	1057.2	3.0	6.5	12.3	22.9	13.6	2.2	−4.4	168	−1.6	153	−3.4	3	−0.12	80	115.8	0	0
4	1	0	−1	319.4	13.8	592.3	997.8	3.0	5.5	11.0	20.8	12.3	3.1	−4.4	1539	−0.4	2671	−1.5	3	−0.07	100	70.5	0	0
5	1	0	−1	335.8	13.6	600.5	1021.3	3.0	5.5	11.7	21.1	12.2	3.3	−4.6	1610	−0.3	3572	−1.5	3	−0.01	100	69.7	0	0
6	1	0	−1	331.4	13.8	621.9	1067.9	3.0	6.3	11.7	21.5	12.7	3.0	−4.4	1519	−0.6	1668	−1.5	4	−0.05	100	77.8	0	0
7	1	0	−1	319.4	15.0	596.1	1000.0	3.0	5.5	10.9	21.3	12.2	3.1	−4.5	1413	−0.4	2746	−1.6	3	−0.07	100	70.8	0	0
8	0	0	−1	335.8	12.2	611.0	1028.0	3.0	5.5	11.9	20.7	12.2	3.3	−4.9	1414	−0.4	3753	−1.6	3	0.00	100	70.8	0	0
9	1	0	−1	331.4	13.0	617.2	1056.2	3.0	6.3	11.6	21.0	12.7	2.9	−4.3	1410	−0.6	1444	−1.5	4	−0.08	100	79.0	0	0
10	0	0	−2	317.4	12.3	595.6	1011.8	4.0	6.3	11.8	22.1	14.5	1.8	−3.8	449	−1.1	447	−2.5	4	−0.24	85	93.5	0	0
11	0	0	−2	301.4	11.8	582.8	980.8	4.0	5.5	11.8	21.3	14.0	1.8	−3.6	410	−1.2	372	−2.4	3	−0.22	84	87.2	0	0
THA [b]	0	0	1	198.3	4.2	430.7	709.9	1.5	2.0	6.9	10.7	6.4	2.6	−3.1	2931	0.0	1582	−1.8	3	0.07	100	34.2	0	0
AAZ [c]	0	0	−2	222.2	10.9	412.9	634.3	3.0	9.0	6.8	17.6	15.2	−1.8	−1.6	36	−1.8	24	−5.9	1	−0.99	44	133.3	0	0

[a] Various computational pharmacodynamic and pharmacokinetic parameters of synthesized compounds in this research were predicted such as number of property or descriptor values that fall outside the 95% range of similar values for known drugs. (#stars; 0–5), number of reactive functional groups (#rtvFG; 0–2), central nervous system activity (CNS; −2 inactive, +2 active), molecular weight of the compound (MW; 130.0 - 725.0), computed dipole moment of the compound (Dipole; 1.0 - 12.5), total solvent accessible surface area (SASA; 300.0 - 1000.0), total solvent-accessible volume in cubic angstroms using a probe with a 1.4 Å Radius (Volume; 500.0 - 2000.0), number of hydrogen bonds that would be donated by the solute to water molecules in an aqueous solution (donorHB; 0.0 - 6.0), number of hydrogen bonds that would be accepted by the solute from water molecules in an aqueous solution (accptHB; 2.0 - 20.0), hexadecane/gas partition coefficient (QPlogPC16; 4.0 - 18.0), octanol/gas partition coefficient (QPlogPoct; 8.0 - 35.0), water/gas partition coefficient (QPlogPw; 4.0 - 45.0), octanol/water partition coefficient (QPlogPo/w; −2.0 - 6.5), aqueous solubility (QPlogS; −6.5 - 0.5), apparent Caco-2 cell permeability in nm/sec (QPPCaco; <25 poor, great >500), brain/blood partition coefficient (QPlogBB; −3.0 - 1.2), apparent MDCK cell permeability in nm/sec (QPPMDCK; <25 poor, great >500), skin permeability (QPlogKp; −8.0 - −1.0), number of likely metabolic reactions (#metab; 1–8), prediction of binding to human serum albumin (QPlogKhsa; −1.5 - 1.5), human oral absorption (HOA; <25% poor, high >80%), van der Waals surface area of polar nitrogen and oxygen atoms (PSA; 7.0 - 200.0), number of violations of Lipinski's rule of five (max. 4), and number of violations of Jorgensen's rule of three (max. 3). [b] Tacrine. [c] Acetazolamide.

Enzyme inhibition assay

AChE and hCAs activity assay

In the present study, AChE from *Electrophorus electricus* (Sigma C2888, Type V- S) were purchased from Sigma-Aldrich Chemie GmbH. *In vitro* effects on AChE activity of the novel synthesized thiosemicarbazones derivatives (**1**–**11**) and reference compound tacrine (THA) were evaluated by the method of Ellman et al.[43] as described in detail.[44] Results were performed spectrophotometrically at 412 nm using AChI. The inhibition effects of these thiosemicarbazones (**1**–**11**) and reference compound, acetazolamide (AAZ) versus the esterase activity of the *h*CAs were determined by following the change in absorbance at 348 nm according to the assay defined by Verpoorte et al.[45] as describe in prior studies.[46] *h*CAs's activities were measured using 4-nitrophenyl acetate as previous studies.[47] All the measurements were repeated thrice.

AChE and hCAs kinetic assay

To investigate the *in vitro* inhibitory mechanisms of the novel synthesized thiosemicarbazones derivatives (**1**–**11**), kinetic studies were made with the variable compound and substrate concentrations. IC_{50} and Lineweaver-Burk curves[48] were generated as previously reported in the previous studies.[49] From the observed data, IC_{50} and K_I values for these derivatives were computed, and the types of inhibition of AChE and *h*CAs were determined.[50]

DFT calculation procedure

Gaussian 09 software[51] was used for the DFT[52] calculations performed to examine both the spectroscopic and electronic properties of the compounds. The compounds were optimized to the ground state energies corresponding to global minimum energy points on the potential energy surface, in the gas phase, using the B3LYP/6-311++G(2d,2p) level of theory, and this was supported by the absence of imaginary frequency modes in the IR calculations.

The optimization and spectral data acquisition processes of the ^{1}H and ^{13}C-NMR calculations were carried out in the dimethyl sulfoxide (DMSO) phase, in accordance with the experiments. The Gauge-independent atomic orbital (GIAO) method was used for the calculations, with the conductor-like polarizable continuum model (CPCM) included to take solvent effects into account. Relative chemical shifts were obtained by subtracting the absolute chemical shielding values calculated in the DMSO phase at B3LYP/6-311++G(2d,2p) level for the proton (31.8149 ppm) and carbon (183.737 ppm) of tetramethylsilane (TMS).

Global chemical reactivity parameters such as HOMO-LUMO band gap (E_g), electronegativity (χ), electrophilic (ω) and nucleophilic index (ε), electro accepting (ω^{+}) and electrodonating power (ω^{-}) were calculated using the frontier molecular orbital (FMO) energy eigenvalues obtained from the calculations performed, in gas phase, at the same level of theory. QTAIM[53] calculations and IRI[54] visualization data were obtained using Multiwfn software.[37]

Molecular docking study

This research used the Small-Molecule Drug Discovery Suite for Mac, version 2023-1, to conduct a molecular docking analysis. The protein data bank (PDB) IDs 1AZM,[55] 3HS4,[56] and 7XN1[57] representing *h*CA I and II isoforms and AChE were obtained from the RCSB Protein Data Bank and used as models. The Protein

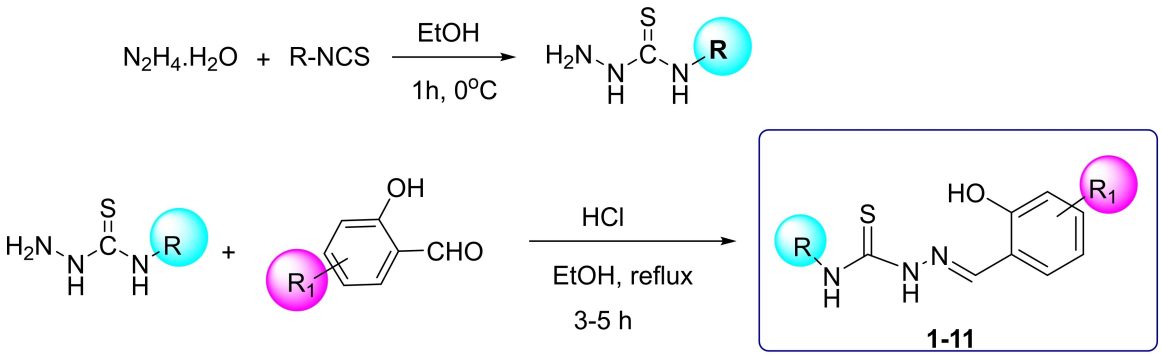

1, R= $PhCH_2$, R_1= 3-OMe
2, R= 4-CH_3-Ph, R_1= 3-OMe
3, R= 4-NO_2-Ph, R_1= 3-OMe
4, R= 2-F-Ph, R_1= 3-OMe
5, R= 2-Cl-Ph, R_1= 3-OMe
6, R= 2-OMe-Ph, R_1= 3-OMe
7, R= 3-F-Ph, R_1= 3-OMe
8, R= 3-Cl-Ph, R_1= 3-OMe
9, R= 3-OMe-Ph, R_1= 3-OMe
10, R= 2-OMe-Ph, R_1= 4-OH
11, R= $PhCH_2$, R_1= 4-OH

Scheme 2. Synthesis route of new thiosemicarbazones (**1**-**11**).

Preparation Wizard[58] of the Small-Molecule Drug Discovery Suite was used to prepare these structures for docking. The ChemDraw program, version 21 for Mac, was used to sketch the structures of novel thiosemicarbazones bearing Schiff-bases (**1**-**11**), which were then optimized using the LigPrep module[59] of the same software program at pH 7.4 ± 0.5 in the optimal potential liquid simulations 4 (OPLS4) force field with Epik.[60] The SiteMap tool[61] was also used to identify the active site residues defined in the Receptor Grid Generation module[62] to generate the receptor grid in the Maestro panel. The Glide application[63] was used with default settings and the extra precision (XP) method[64] to dock ligands to *h*CAs and AChE. The efficacy of the Prime MM-GBSA[65] in predicting relative binding affinity in the VSGB energy model and OPLS4 force field was assessed using the protein-ligand complexes 1AZM, 3HS4, and 7 N3I. Furthermore, the QikProp tool[66] was employed to predict the ADME characteristics of all targeted compounds (**1**–**11**).

Author Contributions

Musa Erdoğan: Investigation, Spectral analysis, Writing–Review. M. Serdar Çavuş: Investigation, Validation, Writing–Review. Halit Muğlu: Investigation, Methodology, Writing–Review. Hasan Yakan: Investigation, Writing–Review, Visualization & Editing. Cüneyt Türkeş: Conceptualization, Methodology, Formal analysis, Validation, Investigation, and Writing. Yeliz Demir: Conceptualization, Methodology, Formal analysis, Validation, Investigation, and Writing. Şükrü Beydemir: Conceptualization, Methodology, and Funding acquisition.

Acknowledgements

This work was supported by the Research Fund of Anadolu University (grant number 2102 S003). The DFT calculations reported in this article were partially performed at TUBITAK ULAKBIM, High Performance and Grid Computing Center (TRUBA resources).

Conflict of Interests

The authors declare no conflict of interest.

Data Availability Statement

The data that support the findings of this study are available from the corresponding author upon reasonable request.

Keywords: DFT · enzyme inhibition · molecular docking · structure characterization · thiosemicarbazones

[1] A. Cinarli, D. Gürbüz, A. Tavman, A. S. Birteksöz, *Bull. Chem. Soc. Ethiop.* **2011**, *25*, 407–417.
[2] S. Pandeya, D. Sriram, G. Nath, E. De Clercq, *Pharm. Acta Helv.* **1999**, *74*, 11–17.
[3] H. Yakan, Ü. M. Koçyiğit, H. Muğlu, M. Ergul, S. Erkan, E. Güzel, P. Taslimi, İ. Gülçin, *J. Biochem. Mol. Toxicol.* **2022**, *36*, e23018.
[4] S. Alyar, T. Şen, Ü. Ö. Özmen, H. Alyar, Ş. Adem, C. Şen, *J. Mol. Struct.* **2019**, *1185*, 416–424.
[5] M. Verma, S. N. Pandeya, K. N. Singh, J. P. Stables, *Acta Pharmaceutica* **2004**, *54*, 49–56.
[6] T. Aboul-Fadl, F. A. S. Bin-Jubair, O. Aboul-Wafa, *European J. Medicinal Chemistry* **2010**, *45*, 4578–4586.
[7] S. Shukla, R. S. Srivastava, S. K. Shrivastava, A. Sodhi, P. Kumar, *Med. Chem. Res.* **2013**, *22*, 1604–1617.
[8] S. S. Ali, E.-R. Kenawy, F. I. Sonbol, J. Sun, M. Al-Etewy, A. Ali, L. Huizi, N. A. El-Zawawy, *Pharm. Res.* **2018**, *36*, 5.
[9] a) H. Muğlu, H. Yakan, A. G. A. Misbah, M. S. Çavuş, T. K. Bakır, *Res. Chem. Intermed.* **2021**, *47*, 4985–5005; b) H. Muğlu, H. Yakan, T. K. Bakir, *Turk. J. Chem.* **2020**, *44*, 237–248.
[10] S. Chigurupati, *J. Med. Bioeng.* **2015**, *4*, 363–366.

[11] V. Mishra, S. N. Pandeya, E. DeClercq, C. Pannecouque, M. Witvrouw, *Pharm. Acta Helv.* **1998**, *73*, 215–218.
[12] M. Tahriri, M. Yousefi, K. Mehrani, M. Tabatabaee, M. D. Ashkezari, *Pharm. Chem. J.* **2017**, *51*, 425–428.
[13] A. Karaküçük-İyidoğan, D. Taşdemir, E. E. Oruç-Emre, J. Balzarini, *European J. Medicinal Chemistry* **2011**, *46*, 5616–5624.
[14] B. N. Brousse, R. Massa, A. G. Moglioni, M. Martins Alho, G. Gutkind, G. Y. Moltrasio, *J. the Chilean Chemical Society* **2004**, *49*, 45–49.
[15] N. Karali, A. Gürsoy, *Farmaco (Societa chimica italiana: 1989)* **1994**, *49*, 819–822.
[16] U. Kulandaivelu, V. G. Padmini, K. Suneetha, B. Shireesha, J. V. Vidyasagar, T. R. Rao, J. K N, A. Basu, V. Jayaprakash, *Arch. Pharm.* **2011**, *344*, 84–90.
[17] H. Pervez, N. Manzoor, M. Yaqub, A. Khan, K. M. Khan, F.-u.-H. Nasim, M. I. Choudhary, *Lett. Drug Des. Discovery* **2010**, *7*, 102–108.
[18] N. P. Prajapati, K. D. Patel, R. H. Vekariya, H. D. Patel, D. P. Rajani, *J. Mol. Struct.* **2019**, *1179*, 401–410.
[19] Z. Bakherad, M. Safavi, A. Fassihi, H. Sadeghi-Aliabadi, M. Bakherad, H. Rastegar, M. Saeedi, J. B. Ghasemi, L. Saghaie, M. Mahdavi, *Chem. Biodiversity* **2019**, *16*, e1800470.
[20] H. Yakan, *Turk. J. Chem.* **2020**, *44*, 1085–1099.
[21] A. R. Božić, N. Filipović, I. Novaković, S. Bjelogrlić, J. B. Nikolić, S. Z. Drmanić, A. D. Marinković, *J. the Serbian Chemical Society* **2017**, *82*, 495–508.
[22] K. H. D. Reddy, S.-M. Lee, K. Seshaiah, R. K. Babu, *J. the Serbian Chemical Society* **2013**, *78*, 229–240.
[23] a) M. Yiğit, Y. Demir, D. Barut Celepci, T. Taskin-Tok, A. Arınç, B. Yiğit, M. Aygün, İ. Özdemir, İ. Gülçin, *Arch. Pharm.* **2022**, *355*, 2200348; b) S. Bilginer, S. K. Bardaweel, Y. Demir, I. Gulcin, C. Kazaz, *Med. Chem. Res.* **2022**, *31*, 925–935.
[24] a) M. Hamide, Y. Gök, Y. Demir, G. Yakalı, T. T. Tok, A. Aktaş, R. Sevinçek, B. Güzel, İ. Gülçin, *J. Mol. Struct.* **2022**, *1265*, 133266; b) M. S. Özaslan, R. Sağlamtaş, Y. Demir, Y. Genç, İ. Saraçoğlu, İ. Gülçin, *Chem. Biodiversity* **2022**, *19*, e202200280.
[25] N. Oztaskin, S. Goksu, Y. Demir, A. Maras, İ. Gulcin, *Molecules* **2022**, *27*, 7426.
[26] M. Hamide, Y. Gök, Y. Demir, R. Sevinçek, T. Taskin-Tok, B. Tezcan, A. Aktaş, İ. Gülçin, M. Aygün, B. Güzel, *Chem. Biodiversity* **2022**, *19*, e202200257.
[27] I. Mahmudov, Y. Demir, Y. Sert, Y. Abdullayev, A. Sujayev, S. H. Alwasel, I. Gulcin, *Arabian J. Chemistry* **2022**, *15*, 103645.
[28] I. Kraicheva, I. Tsacheva, R. Nikolova, M. Topashka-Ancheva, I. Stoineva, B. Shivachev, *Phosphorus Sulfur Silicon Relat. Elem.* **2017**, *192*, 403–409.
[29] S. Tellamekala, M. Gundluru, S. Sarva, M. R. Nadiveedhi, M. Sudileti, R. Allagadda, A. R. Chippada, S. R. Cirandur, *Synth. Commun.* **2019**, *49*, 563–575.
[30] Ö. Demirci, B. Tezcan, Y. Demir, T. Taskin-Tok, Y. Gök, A. Aktaş, B. Güzel, İ. Gülçin, *Molecular Diversity* **2022**.
[31] Y. Demir, C. Türkeş, M. S. Çavuş, M. Erdoğan, H. Muğlu, H. Yakan, Ş. Beydemir, *Arch. Pharm.* **2023**, *356*, 2200554.
[32] H. Yakan, H. Muğlu, C. Türkeş, Y. Demir, M. Erdoğan, M. S. Çavuş, Ş. Beydemir, *J. Mol. Struct.* **2023**, *1280*, 135077.
[33] R. J. Obaid, E. U. Mughal, N. Naeem, M. M. Al-Rooqi, A. Sadiq, R. S. Jassas, Z. Moussa, S. A. Ahmed, *Process Biochem.* **2022**, *120*, 250–259.
[34] M. Ishaq, P. Taslimi, Z. Shafiq, S. Khan, R. Ekhteiari Salmas, M. M. Zangeneh, A. Saeed, A. Zangeneh, N. Sadeghian, A. Asari, H. Mohamad, *Bioorg. Chem.* **2020**, *100*, 103924.
[35] a) M. Elkolli, N. Chafai, S. Chafaa, I. Kadi, C. Bensouici, A. Hellal, *J. Mol. Struct.* **2022**, *1268*, 133701; b) N. Dawar, J. Devi, B. Kumar, A. Dubey, *Inorg. Chem. Commun.* **2023**, *151*, 110567; c) R. Arshad, M. A. Khan, S. Mutahir, S. Hussain, G. H. Al-Hazmi, M. S. Refat, *Polycyclic Aromat. Compd.* **2023**, *43*, 6750–6765; d) N. Mani, D. Nicksonsebastin, M. Prasath, *Chemical Physics Impact* **2023**, *7*, 100292; e) K. Saranya, S. Murugavel, *J. Mol. Struct.* **2021**, *1229*, 129487; f) H. Tlidjane, N. Chafai, S. Chafaa, C. Bensouici, K. Benbouguerra, *J. Mol. Struct.* **2022**, *1250*, 131853.
[36] a) P. Tarasconi, S. Capacchi, G. Pelosi, M. Cornia, R. Albertini, A. Bonati, P. P. Dall'Aglio, P. Lunghi, S. Pinelli, *Bioorg. Med. Chem.* **2000**, *8*, 157–162; b) M. Khalid, R. Jawaria, M. U. Khan, A. A. C. Braga, Z. Shafiq, M. Imran, H. M. A. Zafar, A. Irfan, *ACS Omega* **2021**, *6*, 16058–16065; c) W. A. Arafa, M. G. Badry, *J. Chemical Research* **2016**, *40*, 385–392.
[37] T. Lu, F. Chen, *J. Computational Chemistry* **2012**, *33*, 580–592.
[38] S. Hashmi, S. Khan, Z. Shafiq, P. Taslimi, M. Ishaq, N. Sadeghian, H. S. Karaman, N. Akhtar, M. Islam, A. Asari, H. Mohamad, İ. Gulçin, *Bioorg. Chem.* **2021**, *107*, 104554.
[39] P. Eraslan-Elma, A. Akdemir, E. Berrino, M. Bozdağ, C. T. Supuran, N. Karalı, *Arch. Pharm.* **2022**, *355*, 2200023.
[40] C. A. Lipinski, F. Lombardo, B. W. Dominy, P. J. Feeney, *Adv. Drug Delivery Rev.* **1997**, *23*, 3–25.
[41] E. M. Duffy, W. L. Jorgensen, *J. the American Chemical Society* **2000**, *122*, 2878–2888.
[42] A. Benmohammed, O. Khoumeri, A. Djafri, T. Terme, P. Vanelle, *Molecules* **2014**, *19*, 3068–3083.
[43] G. L. Ellman, K. D. Courtney, V. Andres Jr, R. M. Featherstone, *Biochem. Pharmacol.* **1961**, *7*, 88–95.
[44] M. Kalaycı, C. Türkeş, M. Arslan, Y. Demir, Ş. Beydemir, *Arch. Pharm.* **2021**, *354*, 2000282.
[45] J. A. Verpoorte, S. Mehta, J. T. Edsall, *J. Biol. Chem.* **1967**, *242*, 4221–4229.
[46] Ü. Yaşar, İ. Gönül, C. Türkeş, Y. Demir, Ş. Beydemir, *ChemistrySelect* **2021**, *29*, 7278–7284.
[47] C. Türkeş, M. Arslan, Y. Demir, L. Cocaj, A. R. Nixha, Ş. Beydemir, *Bioorg. Chem.* **2019**, *89*, 103004.
[48] H. Lineweaver, D. Burk, *J. the American Chemical Society* **1934**, *56*, 658–666.
[49] a) B. Sever, C. Türkeş, M. D. Altıntop, Y. Demir, G. A. Çiftçi, Ş. Beydemir, *Arch. Pharm.* **2021**, *354*, 2100294; b) S. Askin, H. Tahtaci, C. Türkeş, Y. Demir, A. Ece, G. A. Çiftçi, Ş. Beydemir, *Bioorg. Chem.* **2021**, *113*, 105009; c) Y. Demir, H. Ceylan, C. Türkeş, Ş. Beydemir, *J. Biomol. Struct. Dyn.* **2022**, *40*, 12008–12021; d) G. Yapar, H. Esra Duran, N. Lolak, S. Akocak, C. Türkeş, M. Durgun, M. Işık, Ş. Beydemir, *Bioorg. Chem.* **2021**, *117*, 105473; e) C. Türkeş, Y. Demir, Ş. Beydemir, *ChemistrySelect* **2021**, *6*, 11915–11924; f) C. Türkeş, A. Ö. Kesebir, Y. Demir, Ö. İ. Küfrevioğlu, Ş. Beydemir, *ChemistrySelect* **2021**, *6*, 11137–11143; g) B. Çalışkan, Y. Demir, C. Türkeş, *Biotechnol. Appl. Biochem.* **2022**, *69*, 2273–2283.
[50] a) C. Türkeş, Y. Demir, Ş. Beydemir, *J. Biomol. Struct. Dyn.* **2021**, *39*, 1672–1680; b) B. Sever, C. Türkeş, M. D. Altıntop, Y. Demir, Ş. Beydemir, *International J. Biological Macromolecules* **2020**, *163*, 1970–1988.
[51] M. Frisch, G. Trucks, H. Schlegel, G. Scuseria, M. Robb, J. Cheeseman, G. Scalmani, V. Barone, B. Mennucci, G. Petersson, *See also: URL: http://www. gaussian. Com***2009**.
[52] a) P. Hohenberg, W. Kohn, *B864* **1964**; b) W. Kohn, L. J. Sham, *Phys. Rev.* **1965**, *140*, A1133.
[53] a) R. F. W. Bader, *Acc. Chem. Res.* **1985**, *18*, 9–15; b) R. F. W. Bader, *Chem. Rev.* **1991**, *91*, 893–928.
[54] T. Lu, Q. Chen, *Chemistry–Methods* **2021**, *1*, 231–239.
[55] S. Chakravarty, K. K. Kannan, *J. Mol. Biol.* **1994**, *243*, 298–309.
[56] K. H. Sippel, A. H. Robbins, J. Domsic, C. Genis, M. Agbandje-McKenna, R. McKenna, *Acta Crystallogr. Sect. F* **2009**, *65*, 992–995.
[57] K. V. Dileep, K. Ihara, C. Mishima-Tsumagari, M. Kukimoto-Niino, M. Yonemochi, K. Hanada, M. Shirouzu, K. Y. J. Zhang, *Int. J. Biol. Macromol.* **2022**, *210*, 172–181.
[58] a) Schrödinger Release 2023–1: Protein Preparation Wizard, Schrödinger, LLC, New York, NY, 2023; b) A. Buza, C. Türkeş, M. Arslan, Y. Demir, B. Dincer, A. R. Nixha, Ş. Beydemir, *Int. J. Biol. Macromol.* **2023**, *239*, 124232.
[59] a) Schrödinger Release 2023–1: LigPrep, Schrödinger, LLC, New York, NY, 2023; b) D. Osmaniye, C. Türkeş, Y. Demir, Y. Özkay, Ş. Beydemir, Z. A. Kaplancıklı, *Archiv der Pharmazie* **2022**, *355*, 2200132.
[60] a) Schrödinger Release 2023–1: Epik, Schrödinger, LLC, New York, NY, 2023; b) J. C. Shelley, A. Cholleti, L. L. Frye, J. R. Greenwood, M. R. Timlin, M. Uchimaya, *J. Comput.-Aided Mol. Des.* **2007**, *21*, 681–691.
[61] a) Schrödinger Release 2023–1: SiteMap, Schrödinger, LLC, New York, NY, 2023; b) T. A. Halgren, *J. Chem. Inf. Model.* **2009**, *49*, 377–389.
[62] a) Schrödinger Release 2023–1: Receptor Grid Generation, Schrödinger, LLC, New York, NY, 2023; b) N. Lolak, S. Akocak, M. Durgun, H. E. Duran, A. Necip, C. Türkeş, M. Işık, Ş. Beydemir, *Mol. Diversity* **2022**. *27*, 1735–1749.
[63] a) Schrödinger Release 2023–1: Glide, Schrödinger, LLC, New York, NY, 2023; b) S. A. Güngör, M. Köse, M. Tümer, C. Türkeş, Ş. Beydemir, *J. Biomol. Struct. Dyn.* **2022**, 1–11; c) Ö. Güleç, C. Türkeş, M. Arslan, Y. Demir, B. Dincer, A. Ece, Ş. Beydemir, *J. Biomolecular Structure and Dynamics* 1–19. https://doi.org/10.1080/07391102.2023.2240889
[64] a) R. A. Friesner, J. L. Banks, R. B. Murphy, T. A. Halgren, J. J. Klicic, D. T. Mainz, M. P. Repasky, E. H. Knoll, M. Shelley, J. K. Perry, D. E. Shaw, P. Francis, P. S. Shenkin, *J. Med. Chem.* **2004**, *47*, 1739–1749; b) T. A. Halgren, R. B. Murphy, R. A. Friesner, H. S. Beard, L. L. Frye, W. T. Pollard, J. L. Banks, *J. Med. Chem.* **2004**, *47*, 1750–1759; c) K. Yararli, E. B. Ozer, S. Bayindir, C. Caglayan, C. Turkes, S. Beydemir, *J. Mol. Struct.* **2023**, *1276*, 134783.

[65] a) Schrödinger Release 2023–1: Prime, Schrödinger, LLC, New York, NY, 2023; b) G. Barreiro, C. R. W. Guimarães, I. Tubert-Brohman, T. M. Lyons, J. Tirado-Rives, W. L. Jorgensen, *J. Chem. Inf. Model.* **2007**, *47*, 2416–2428; c) C. Kakakhan, C. Türkeş, Ö. Güleç, Y. Demir, M. Arslan, G. Özkemahlı, Ş. Beydemir, *Bioorg. Med. Chem.* **2023**, *77*, 117111.

[66] a) Schrödinger Release 2023–1: QikProp, Schrödinger, LLC, New York, NY, 2023; b) L. Ioakimidis, L. Thoukydidis, A. Mirza, S. Naeem, J. Reynisson, *QSAR Comb. Sci.* **2008**, *27*, 445–456; c) Ö. Güleç, C. Türkeş, M. Arslan, Y. Demir, Y. Yeni, A. Hacımüftüoğlu, E. Ereminsoy, Ö. İ. Küfrevioğlu, Ş. Beydemir, *Mol. Diversity* **2022**, *26*, 2825–2845.

Manuscript received: July 20, 2023
Accepted manuscript online: September 28, 2023
Version of record online: October 23, 2023